ROCKFALL SUSCEPTIBILITY MAPS FOR NEW MEXICO

New Mexico Bureau of Geology and Mineral Resources Open-file Report 595

December, 2017

Prepared by

Daniel J. Koning, *Senior Field Geologist*

Mark Mansell, *GIS Analyst*

New Mexico Bureau of Geology and Mineral Resources
New Mexico Institute of Mining and Technology
New Mexico Tech, 801 Leroy Place
Socorro, NM 87801

Prepared for

New Mexico Department of Homeland Security and Emergency Management
13 Bataan Blvd.
Santa Fe, NM 87508

New Mexico Hazard Mitigation Assistance Program

Sub-grant FEMA-4152-DR-NM-020

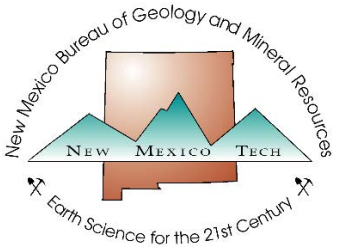

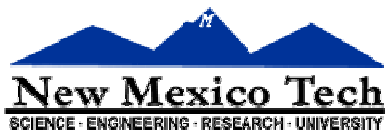

ACKNOWLEDGEMENTS

The authors thank the members of the New Mexico Department of Homeland Security and Emergency Management Preparedness Bureau for their assistance and guidance in this investigation, particularly Wendy Blackwell, State Hazard Mitigation Supervisor, and Kyle Mason, Mitigation Specialist. The Earth Data Analysis Center (EDAC) of the University of New Mexico digitized scans of rockfall maps for this project. The U.S. Army Corps of Engineers provided the high-resolution digital terrain model that served as a basis for all topographic data used in this investigation. ESRI provided the GIS software and tools used in processing spatial data throughout this project.

DISCLAIMER

The State of New Mexico assumes no liability of the contents of this report or use thereof.

The contents of this report reflect the views of the authors who are solely responsible for the facts and accuracy of the material presented. The contents do not necessarily reflect the official views of the State of New Mexico or the Department of Homeland Security and Emergency Management.

The State of New Mexico does not endorse products or software. Use of particular products herein was solely for the purpose of completing this project. Trademarks or manufacturers' names appear herein only where and because they are considered essential to the object of this document.

This report does not constitute a standard or specification. This report and accompanying map are not substitutes for detailed, location-specific geotechnical or geohazards analyses.

Contents

Figures

Tables

Plates

Appendices (Digital)

1 Executive Summary

Using a dataset of preexisting mapped landslides, we create two maps that provide a first-order approximation of rockfall susceptibility for the state of New Mexico. In natural hazard assessments, the term 'susceptibility' is used to describe the natural propensity of the landscape to produce a given hazard (in this case, rockfall). In other words, these maps depict the likelihood that a rockfall event will occur in a specified area based on local terrain conditions, given adequate driving forces or destabilizing phenomena.

For the purpose of our analyses, we include rock topples with rock falls. Both phenomena occur when a mass of rock fails on a very steep slope, cliff, or ledge. A period of free-fall may be involved initially, but most of the downslope transport involves bouncing and flying along ballistic trajectories or rolling down a slope (run-out zone). During this process, the rock mass may split into several pieces or evolve into a rock avalanche. Eventually, frictional forces will cause the rolling rock to come at rest, either on a slope or relatively gentle ground.

An essential input for our maps was a preexisting, statewide map of rockfalls produced by Cardinali et al. (1990). This map was made using aerial imagery with limited field checks. Our reconnaissance and field experience indicate this input dataset captures only a fraction of the total rock falls, but nonetheless it is assumed to be a statistically valid subsample of the total. These rock falls were mapped using aerial photography, and thus this subsample probably has a bias towards larger rockfalls (coarse boulders large enough to see on aerial photography).

The first susceptibility map (Plate 1) shows the point densities of the mapped rockfalls of Cardinali et al. (1990), which are contoured using the kernel function. Its usefulness is limited, however, given that only a small percentage of the total rock falls are actually mapped. However, it probably does serve as a proxy for where large rockfall events may occur in the future.

Another rockfall susceptibility map (Plate 2) was constructed to capture a greater range of rockfall sizes. This method relates mapped rock falls (Cardinali et al., 1990) to nearby slope values. Using a 28 m DEM in ARC GIS, a slope map is created. We capture the maximum slope around a mapped rock fall point using a 300 m-radius window, which corresponds to the median of the error range in the mapped rockfall points. The average and maximum value of the slope within this window was obtained, but the frequency distribution curve for the average value is heavily skewed to low values, probably because most of New Mexico is relatively flat and spatial errors would result in a rockfall being on low-sloping ground. However, the maximum value within the window gave a quasi-normal distribution centered on a mean value of 29° and having a standard deviation of 12°. We chose to use these maximum values within the 300 m-radius window, with the assumption that most rock falls tend to accumulate on relatively steep talus slopes.

Using the mean and standard deviations calculated from the distribution of these maximum slopes, we categorize the aforementioned slope map into three classes (corresponding to map zones) that relate to rockfall susceptibility. "Likely susceptible" zones correspond to slopes lying at or above the mean-less-one standard-deviation (17°). In this zone are local areas (over approximate distances of 300-1000 m) containing ledges or cliffs that could generate

rockfalls, and slopes may be sufficiently steep to allow rockfall transport over various distances. "Potentially susceptible" zones correspond to slopes in the range of 8-17°, bracketed by the mean-less-one standard-deviation and the 5th percentile of the aforementioned maximum slope frequency distribution. In a "potentially susceptible" zone, there could possibly be rockfall-producing ledges not captured by the 28 m DEM. This susceptibility zone also includes a 470 m buffer extending downslope (on 5-17° sloping topographic surfaces) of high susceptibility areas, designed to capture rockfalls that have sufficient momentum to travel notably downhill of Likely susceptible areas (≥17° slopes) onto slopes that could correspond to proximal reaches of bouldery alluvial fans (~5°). The 470 m distance value corresponds to the 90th percentile (excluding outliers) of mapped rockfall distances from the high-susceptibility zone. "Unlikely susceptible" zones include very low slopes (<8°) lying outside of the aforementioned buffer. Final processing steps consisted of down-sampling to 500 m grid-size consistent with a 1:750,000 final map scale.

We prefer the second map (Plate 2), conservatively constructed using slope-defined susceptibility boundaries, as the more adequate representation of rockfall susceptibility because it incorporates a wider range of rockfall sizes than the rockfall susceptibility map shown in Plate 1. Neither of the maps (Plates 1 and 2) contain information on the potential for adequate driving forces to occur, nor do they contain information on the frequency at which adequate driving forces may occur, and hence are not a complete hazard maps. The maps are intended for use at a spatial scale of 1:750,000 for regional planning purposes and for determining where more detailed studies may be warranted. In the absence of other data regarding rockfall intensity (i.e., kinetic energy) and event frequency, the maps alone are not adequate for risk assessment nor site-specific assessments of rockfall susceptibility. The New Mexico Bureau of Geology and Mineral Resources shall not be liable under any circumstances for any direct, indirect, special, incidental, or consequential damages with respect to claims by users of this product. The views and conclusions presented here should not be interpreted as necessarily representing the official views or policies, either expressed or implied, of the State of New Mexico.

2 Introduction

2.1 Purpose and Funding

This project was initiated in order to better evaluate the potential hazard posed by rockfalls in the state of New Mexico. Maps showing rockfall susceptibility (i.e., where rockfalls could be expected to occur) could serve as a tool to identify regions in the state where rockfall risk should be considered by public and private planners, as well as the NM Department of Transportation. Such maps would also be essential precursors of complete hazard maps, which would incorporate other rockfall parameters such as magnitude (intensity) and frequency of occurrence. These hazard maps could then be folded into risk maps, which incorporate potential costs and societal impacts. The rockfall susceptibility maps presented in this report will also assist the NM Department of Homeland Security in preparing for their 2018 update for the N.M. State Hazard Mitigation plan for FEMA. Funding for this project was obtained via a sub-grant through the NM Department of Homeland Security and Emergency Management (FEMA-4152-DR-NM-020).

2.2 Nature of the hazard

2.2.1 Societal risk

Rockfalls are an important process by which the landscape erodes in mountainous regions, and a dominant mechanism for erosion of cliff faces (e.g., Wieczorek and Jäger, 1996; Kratblatter et al., 2012). Photographs illustrating rockfall are shown in Figure 2.1. Unfortunately, rockfalls also have the potential to create significant damage to human structures or life. Because of their high energy, even relatively small rock falls can pose a substantial hazard. When grouped with larger landslide hazards, the costs of this natural phenomena in the United States alone is thought to be $1-2 billion per year, with >25 associated deaths (https://www.usgs.gov/science/science-explorer/Natural+Hazards). The Yosemite Valley is classic site to illustrate the dangers of rock fall, where documented rock falls occur about 50 times a year (Stock et al., 2013) and two people have died over the past decade.

2.2.2 Recent rockfall incidents in New Mexico

New Mexico has experienced three noteworthy rockfall related incidents in the past two decades. On the east face of Guadalupe Mesa, located west of the Jemez River near the town of San Ysidro, a 150 ft tall and 30 ft-thick rock slab peeled off and broke into numerous boulders that rolled down to the base of the hill (NMDHSEM, 2013). Fortunately, no injuries or damage were reported. The other two incidents occurred along Highway 68 in the Rio Grande Gorge southwest of Pilar. On September 12 of 1988, a falling boulder struck a bus, killing 5 people and injuring 14. On July 25 of 1991, numerous rockfalls and debris flows trapped 20 cars and closed Highway 68 for 19 hours. A 45x15x15 ft crater was created on the road by a 300 ton boulder, and total clean-up costs were ~$75,000 (Haneberg et al., 1992; Haneberg and Bauer, 1993). Photos of 300 ton boulder and its source area are depicted in Figure 2.2.

Figure 2.1. Photographs of various sizes of rock falls. A) Large rockfall blocks at the upper end of the Catwalk near Glenwood, NM. B) Example of the relatively frequent small-size rockfalls that occur in the state. This rockfall, located in the northern Lemitar Mountains, is probably less than 3 months old. C) Recent (<5 years old) rockfall in the Dry Cimmaron Valley. The two white arrows show the source (top, corresponding to the Dakota Sandstone) and the at-rest boulder debris (bottom). Older rockfall boulders litter the slopes. D) Some rockfalls can make it to the canyon floor, but most come to rest on steep slopes (see also photo C). E) Pilar Cliffs alongside NM Highway 68. These serve as the source for rockfalls (cobble to boulder in size) that generally accumulate on steep slopes as scree or talus. Note that roadcuts serve as a secondary source for rockfall (lower left of the photograph), although these generally have lower kinetic energy than rockfalls derived from the upper cliffs.

Figure 2.2. Photographs of "Baby Huey" boulder. This boulder, estimated at 2.7x105 kg (300 ton), slid and bounced down the steep slope flanking the southeast side of U.S. Highway 68, at a location 4.7 km southwest of Pilar (Haneberg and Bauer, 1993). The source of the boulder is shown by the white arrow in the left photograph. This was the most impressive of the numerous rockfalls that occurred on July 25 of 1991. As it bounced down the slope, it created a 45x15x15 ft crater on Highway 68. The boulder's momentum allowed it to travel across the river, where it came to rest on the lower slope (right photos). It was estimated that this boulder was traveling at approximately 21 m/sec and had a total kinetic energy of about 8.5x107 N-m (Haneberg and Bauer, 1993). These rockfalls, in addition to debris flows, trapped 20 cars and closed Highway 68 for 19 hours. Photos courtesy of Paul Bauer (NM Bureau of Geology and Mineral Resources).

2.2.3 Rockfall vs. rock topple

For the purpose of this report on rockfall susceptibility, the process of "rock topple" is included in "rockfall." In a strict sense, however, one may differentiate between the two processes. Rockfall involves downward detachment along a surface where there is minor or little shear displacement (Highland and Bobrowsky, 2008). This surface may correspond with a pre-existing fracture or bedding plane. Rock topple, on the other hand, is when the rock body has forward rotation (out from the slope) about a semi-horizontal axis below the center of gravity of the displaced mass (Highland and Bobrowsky, 2008). Figures 2.3 and 2.4 illustrate the difference between the two processes.

2.2.4 Rockfall processes

Rockfalls are relatively simple to describe and are intuitive to most people. A rock (as small as a pebble or big as a building) falls or rolls down a steep slope or cliff, eventually coming to rest on a shallower slope. Depending on landscape factors, rockfalls can exhibit high mobilities (velocities) and energy. During its transport, a large piece of falling rock may remain intact or shatter into smaller pieces (depending on the degree of acceleration and the strength of the falling rock). An exceptionally large falling rock block that shatters may perhaps evolve into a rock avalanche.

All rockfall events involve the following components: 1) initiation or failure (gravity's force exceeding the tensile strength of the rock, perhaps aided by other processes like freeze thaw), 2) sufficient distance for the rockfall to accelerate (albeit falling or rolling), and 3) resisting forces from objects or friction to cause the rockfall to cease moving. These components relate directly to two spatial zones: 1) source and 2) run-out zone where rockfalls are transported and accumulate. Geomorphic processes or landscape features play an important role in the aforementioned components, and are discussed below.

Slope angle has been argued as the most important independent variable for rockfall hazard assessment (Varnes and IAEG, 1984; Hutchinson, 1995; Moreiras, 2005; Yalcin and Bulut, 2007; Jimenez-Peralvarez et al., 2009; Antoniou and Lekkas, 2010). In the source area, steeper slopes increase the efficacy of gravity and decrease the effective normal forces involved in friction. Steeper slopes also allow a longer transport distance and more time for acceleration. Lastly, decreasing slope angles near the footslope decrease the efficacy of gravity. Furthermore, lower slope angles generally allows more infiltration of surface water, typically leading to greater vegetation growth that can decelerate rockfall.

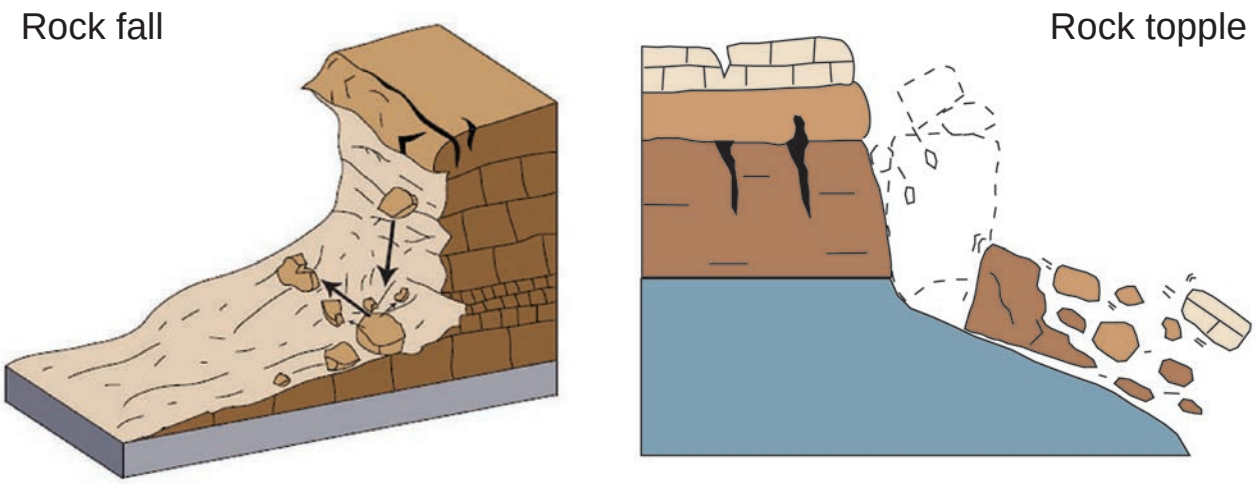

Figure 2.3. Schematic drawings illustrating the difference between rockfall (left, from Highland and Bobrowsky, 2008, who in turn modified it from Cruden and Varnes, 1996) and rock topple (right, from Cruden and Varnes, 1996).

Figure 2.4. Photographs illustrating rock fall vs. rock topple. A) Slab of rock on a vertical face, behind which a deeply penetrating fracture has developed (white arrows). The slab of rock will probably experience rockfall in the near future, where movement will be primarily a downward translation with minimal rotation. Some shear may take place on the aforementioned fracture. B) Fracture density is an important control for rock fall. In Mineral Creek, western Mogollon Mountains, a 1-2 m wide zone of high density fractures has resulted in faster rock fall rates and consequent gully development. C) A 20 m tall (eye estimate) pillar of rock that would have a high propensity for rock topple. In rock topple, the mass of rock rotates forward (away from the slope) about a semi-horizontal axis below the center of gravity of the mass. D) A 5-10 m tall column of rock also having high potential for rock topple in the near future.

Potential driving forces for rockfall mostly include processes that cause bedrock to fracture, which we briefly discuss here. Frost weathering involves freeze/thaw and segregation ice growth. Freeze thaw is associated with water percolating into pore spaces or fractures and then freezing. The ~9% volumetric expansion of the newly formed ice increases tensional stresses at the tips of fractures, facilitating rock breakage. These broken rocks could then fall upon subsequent thawing. Past literature elaborating on this process include Rapp (1960), Church et al. (1979), Davidson and Nye (1985), Coutard and Francou (1989), French (1998), Matsuoka and Sakai (1999), Matsouka (2001), and Macciotta et al. (2015). Segregation ice growth involves migration of water through a frozen fringe to an accreting ice lens, commonly along the interface between rock and ice (Walder and Hallett, 1985; Hallet et al., 1991; Wettlaufer and Worster, 1995; Worster and Wettlaufer, 1999; Rempel et al., 2004). Segregation ice growth begins at subfreezing temperatures (Akagawa and Fukuda, 1991; Hallet et al., 1991), and the stress required to fracture rock is provided by van der Walls and electrostatic forces (Wettlaufer and Worster, 1995; Wilen and Dash, 1995). The efficacy of these two processes, both overall and as a function of rock depth, are dependent on temperature and moisture (Matsuoka and Sakai, 1999; Matsuoka, 2001; Anderson, 1998; Hales and Roering, 2005, 2007; Bathrellos et al., 2014; Boeckli et al., 2011; Fisher et al., 2006; Silhan et al., 2011). Aspect will influence the temperature and effective moisture at a given site, making it a potential factor in the susceptibility of a site to rockfall (e.g., Corò et al., 2015).

Fracture processes relevant for arid regions include dirt cracking, cracking related to solar insolation, and salt weathering. Dirt cracking involves precipitation of laminar calcrete and expansion + contraction of expansive clays in a pre-existing fracture (Doorn, 2011). The importance of insolation-related thermal stresses in rock cracking continues to be debated (e.g., Griggs, 1936; Boelhowers and Jonnson, 2013; Gouide, 2013; Hall and Thorn, 2014). Recent studies have noted crack orientations patterns consistent with solar insolation effects (McFadden et al. (2005) and interpret that solar insolation can be of sufficient magnitude to facilitate incremental crack growth (Moores et al., 2008; Collins and Stock, 2016; Eppes et al., 2017), with temperature perturbation by storms or other weather events playing an important role (Eppes et al., 2016), and these cracks can then be enlarged by other chemical and physical processes. Salt weathering can generate cracks in rocks (Wellman and Wilson, 1965; Yaalon, 1970; Amit et al., 1993; Grossi et al., 2011) or fire (Dragovich, 1993; Bloom, 1998).

Driving forces for rockfall not related to bedrock fracturing include earthquake acceleration, precipitation, and rockfalls generated by large animals. Ground acceleration associated with earthquakes can obviously be an important driver for rockfalls. For example, Adams (1980) noted that rockfall activity is concentrated near earthquake epicenters and decays with distance. Intense precipitation is empirically correlated with rockfall incidences (Luckmann, 1976; Sanderson et al., 1996; Krautblatter and Moser, 2009). One reason for this correlation is debris mobilization from intermediate storage areas on rock faces due surface runoff, including hyperconcentrated flows and debris flows (Fryxell and Horberg, 1943; Berti et al., 1999; Krautblatter and Moser, 2009). Intense rainfall may also increase soil pore pressure and erosion of cohesive soils (Hoek, 2007). Rockfalls generated by large animals may be comparably rare compared to these physical processes, but has been observed first-hand by the lead author several times in the field.

In rockfall source areas, vegetation can be both a resisting and a driving force. Dense root systems can help hold bedrock together, especially in well-vegetated and warmer terrains (Miller and Dunne, 1996; Pachauri and Pant, 1992; Nagarajan et al., 2000). However, relatively sparse and large roots occupying fractures can create expansion (Gökçeoglu and Aksoy, 1996; Yalcin and Bulut, 2007).

Source-area rockfalls are influenced by lithologic factors, especially rock hardness and fracture density (Fischer et al., 2006 and 2012; Pachauri and Pant, 1992; Antoniuou and Lekkas, 2010; Jiménez-Perálvarez et al., 2009, 2011; Yalcin and Bulut, 2007; Coro et al., 2015). Hard rocks create ledges, cliffs, or steep slopes that are necessary for rockfalls. In contrast, weaker rocks tend to form low-angle slopes. The continuity and density of factures is also dependent on rock type and can be formed by a variety of geologic processes (Gudmundsson, 2011). Fractures or bedding planes that have a strong component of dip parallel to the overlying slope have a higher likelihood of being failure planes during a rockfall event. Weathering of these discontinuities can produce clay within fractures, which lower frictional resistance and can expand upon wetting.

During transport, the energy lost by rockfall blocks is a complex function of the block itself, slope characteristics, and roughness. Relevant factors affecting the block are its geomechanical properties, shape, and size. Important features of the slope to consider are its geometry at both macro-topographic (concavity , convexity, gullying) and micro-topographic scales (Frattini et al., 2008). Roughness is a function of the aforementioned slope characteristics, the unconsolidated debris on the slope (e.g., talus), and the protective effect of woody vegetation (e.g., Herwig Proske and Bauer, 2016).

2.3 Susceptibility related to hazard and risk analysis

Susceptibility mapping does not equate with a full hazards map, but rather depicts where a particular hazard is more likely to occur. Conceptually, susceptibility is the propensity of features inherent in the landscape to produce a hazard. It is the likelihood that a rockfall event will occur in a specific area based on local terrain conditions (Brabb, 1984). Susceptibility does not consider driving forces (e.g., precipitation or earthquake acceleration) nor does it include information related to frequency of occurrence. Susceptibility is an integral component, however, of a complete rockfall hazard assessment, which includes the following components: 1) where a hazard is likely to occur, 2) the magnitude of the hazard, 3) frequency of occurrence, and 4) the trajectory and maximum run-out of falling blocks (Ferrari et al., 2016). A complete risk analysis would incorporate both the hazard analysis and societal impacts related to a hazard (i.e., costs, injuries, and deaths).

2.3.1 Regional hazard characterization studies

Most rockfall mapping is at relatively high (detailed) scales, encompassing areas ranging from hillslopes to a drainage basin. Two methods are particularly common at these scales. The first entails computer modeling the steepness and roughness of slopes (e.g., Marquínez et al., 2003; Wang et al., 2014), including the protective or dampening effects of vegetation (e.g., Herwig Proske and Bauer, 2016; Fernandez-Hernández et al., 2011). The second involves

qualitative ranking systems of various slope or rock attributes, which is particularly popular for roadside rockfall studies (see summary in Ferrari et al., 2016). It is difficult to extrapolate slope-dependent deterministic or modeling methods developed at a local scale to a regional scale, because factors controlling slope stability and run-out distances are often not applicable over large areas (e.g., Aleotti and Chowdhury, 1999).

Approaches to regional rockfall mapping typically employ geomorphological mapping (e.g., Reichenbach et al., 2005), statistical, or heuristic methods; numerical modeling has also been attempted (e.g., Acosta et al., 2003). Common statistical methods, which sometimes also involve modeling of runout distances (although this is probably unrealistic for regional scales, Wang et al., 2014), include frequency ratios (Wang et al., 2014), logistic regression (Marquinez et al., 2003), or discriminant analysis (Frattini et al., 2008). These statistical methods provide quantitative estimates of where rockfall should be expected, based on correlating past rockfall events to landscape parameters or driving force parameters. Fernandez-Hernández et al. (2011) used a semi-quantitative, heuristic methodology to create a regional landslide susceptibility map, where they used an index-based overlay method of thematic layers that included slope angle, slope profile curvature, lithology, vegetation cover, and dike density. Many of these studies define slope-angle threshold angles in source areas (Loye et al., 2009: Herwig Proske, 2016; Fernandez-Hernández et al., 2011).

Although statewide landslide susceptibility maps have been created, to the best of our knowledge in the United States there is no statewide susceptibility map specific to rockfall. One statewide landslide map of particular interest in this study is that pertaining to Utah (Giraud and Shaw, 2007). Even though it does not incorporate rockfall, the approach of this work has been followed in our study. This approach involves using pre-existing mapping of landslides and establishing statistic-derived slope-angle thresholds. These statistical methods provide a consistent and relatively objective technique to establish slope-angle boundaries. For each generalized geologic unit, slope values of mapped landslides were compiled. Using the resulting frequency distribution, the average slope angle, range of slope angles, and the standard-deviations are calculated. Slope-angle thresholds are set using the standard-deviation breaks of the frequency distributions. The average landslide slope angle provides a conservative measure of the threshold angle because landslide movements typically result in flatter post-failure slope angles. For normally distributed landslide slope angles, slope-angle thresholds were used to divide the moderate-low and low-very low categories for each geologic unit. One standard deviation was subtracted from the mean slope angle to establish a slope-based boundary between moderate susceptibility and low susceptibility, and slope angles below the mean-minus-two-standard-deviation were assigned a very low susceptibility.

2.3.2 Statewide rockfall mapping in New Mexico

In the 1980s, reputable landslide workers from the U.S. Geological Survey and Italy made a series of regional maps relating to shallow landslides + debris flows, deep-seated landslides, locations of escarpments, and rock falls. These maps were released, at a scale of 1:500,000, as a U.S. Geological Survey open-file report (Cardinali et al., 1990). Motivations for this project included: 1) paucity of information about landslide processes in arid and semi-arid regions of the United States and Italy; 2) a desire to explore techniques for displaying landslide information at small (broad) scales; 3) verification of the time needed to prepare landslide

inventory maps at a small scale for an entire state; and 4) the availability of a statewide inventory of aerial photography (from the New Mexico Bureau of Mines and Mineral Resources and the New Mexico State Highway Department). The northwest part of the state was mapped in 1985-1987. The remainder of the state was largely done between October of 1989 and February of 1990. Mapping was conducted using systematic evaluation of aerial photography across the state and plotting identified landslide-related features (including rockfall) on 1:100,000 base maps. Limited field checking occurred in 1987.

This previous mapping effort utilized two sets of aerial photographs (Cardinali et al., 1990). The northwest part of the state was primarily mapped using black-and-white photos from flights flown in 1953 and 1954 by the Army Map Service (scale of 1:31,500). Color infra-red photographs, from flights flown in 1982 and 1983 under the auspices of the National High Altitude Program (NHAP), were used for the rest of the state (Cardinali et al., 1990). The resolution of the NHAP photography is 3-5 ft. Although Cardinali et al. (1990) do not directly discuss how this resolution relates to mapping to rockfall blocks, we infer that rockfalls <3 m diameter would likely not be readily distinguishable. These authors do state that rock falls and topples are probably under-represented on their maps. In general, in historical rockfall datasets there tends to be a bias towards larger events (Budetta and Nappi, 2013).

Mapped landslide features on the 1:100,000 scale maps were reduced photographically to 1:500,00 and then drafted onto a stable mylar base. This mylar base was given to David Love of the N.M. Bureau of Geology and Mineral Resources. It was digitized by the Earth Data Analysis Center (EDAC_ in the Fall of 2016, and the resulting ARC product made available to the N.M. Bureau of Geology and Mineral Resources in December of 2016. It can be downloaded from the EDAC website (http://edac.unm.edu).

We infer a 0-600 m spatial inaccuracy with the mapped rockfalls of Cardinali et al. (1990). Much rockfall in New Mexico is produced by narrow, long, and windy escarpments underlain by hard rocks (commonly sandstone or lava flows). Comparison of these narrow escarpments with mapped rockfalls commonly show rockfalls paralleling the escarpment, but located unreasonably too far away from the foot of the escarpment. Locally, the mapped rockfalls parallel the escarpment but are located on gently sloping terrain above the escarpments shoulder (Figure 2.5). Measuring the distance of the latter set of mapped rockfalls to the scarp shoulder gives the 0-600 m spatial accuracy values, which are consistent with comparison of other rockfalls in the state to likely rockfall-generating sources.

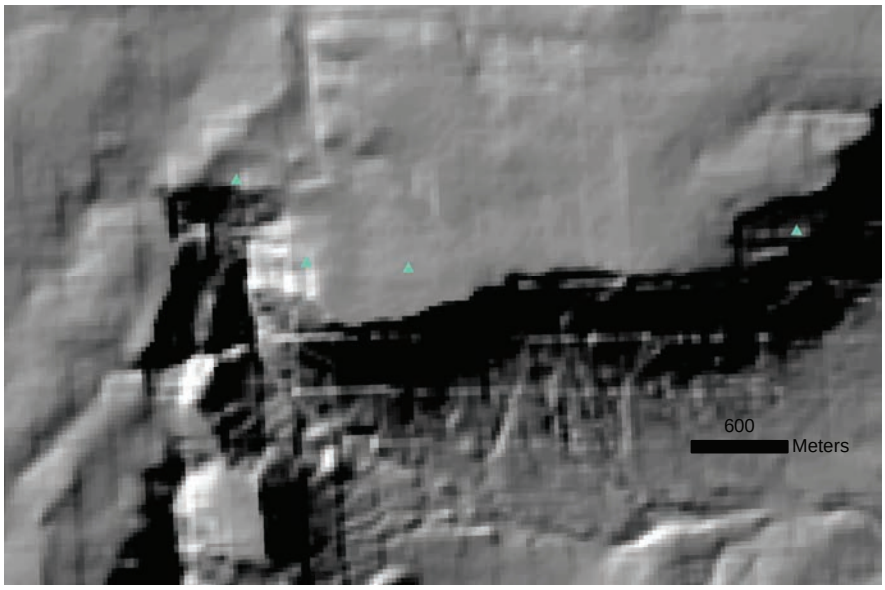

Example of Cardinali et al (1990) mapped rockfalls

Legend

▲ Mapped rock falls

0 0.25 0.5 1 Miles

1:24,000

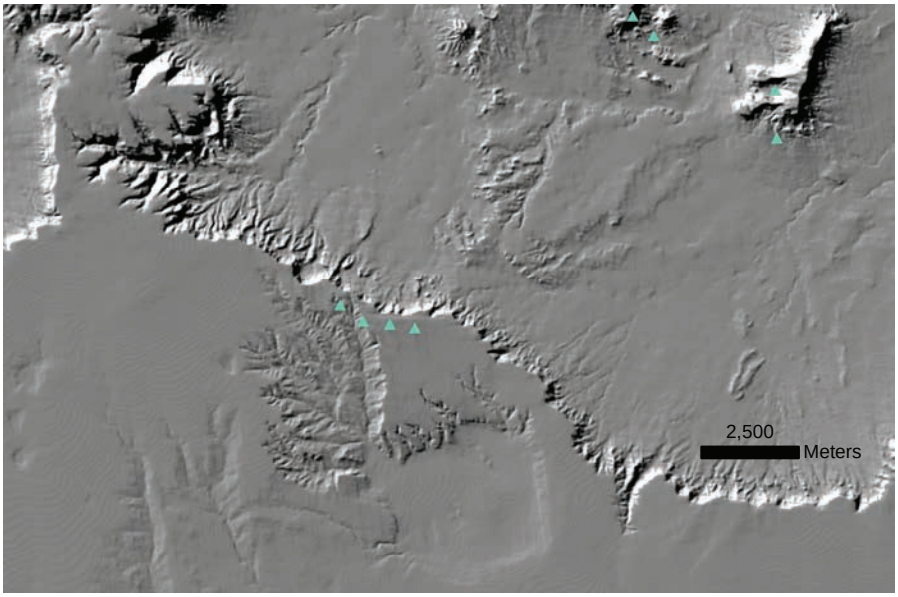

Example of Cardinali et al (1990) mapped rockfalls

Legend

▲ Mapped rock falls

0 1 2 4 Miles

1:100,000

Figure 2.5. Examples of spatial errors in the mapped rockfall points of Cardinali et al. (1990), with a hillshade background. Note that most of these particular rockfall points unrealistically lie on mesa tops above the depicted escarpments. In reality, the should lie on the steep slopes within the escarpment or near the foot of the escarpment. In the lower photograph, note how the rockfalls parallel the top edge of the escarpment. A minimum spatial error could be obtained by measuring the distance from these mapped rockfall points to the toe of the escarpment. Doing this measurement for selected locales across New Mexico suggests a maximum spatial error of 600 m.

3 Methods

To represent rockfall susceptibility maps, two maps were created. Plate 1 contours the densities of previously mapped rockfalls of Cardinali et al. (1990). Plate 2 uses statistically defined slope-angle boundaries to produce a rockfall susceptibility map across the state. The methods relating to each are described below. Note that many factors that are a major influence on rockfall, such as joint density and orientation as well as stratal dips, are not captured on any statewide dataset and so were not incorporated in our work.

3.1 Density contouring of rockfalls in Cardinali et al. (1990)

A map showing the density of mapped rockfalls is of limited usefulness because the input map (Cardinali et al., 1990) under-mapped the rockfalls in New Mexico, as discussed in the previous section. Still, assuming the authors used consistent criteria across the state, such a map may serve as a proxy of rock fall susceptibility. As noted above, the minimum resolution of features that could be observed in the aerial photography is about 3 m. Thus, the map of Cardinali et al. (1990) is biased towards larger rockfalls (>3 m diameter) and any density map constructed from it would represent the density of large-block rockfalls (>3 m diameter). Note that a rockfall density map just shows the run-out zone hazard and does not identify rockfall source areas.

We used the ARC spatial analyst tool called kernel density to calculate a smoothed point density of the mapped landslide points. A kernel density tool calculates the density of features in a specified area around a point or line. It is similar to the spatial analyst tool called point density, but calculates a magnitude-per-unit area using a kernel function. This produces a relatively smooth, tapered surface to each point or line. The following describes how the ARC process works (http://pro.arcgis.com/en/pro-app/tool-reference/spatial-analyst/how-kernel-density-works.htm):

> Conceptually, a smoothly curved surface is fitted over each point. The surface value is highest at the location of the point and diminishes with increasing distance from the point, reaching zero at the search radius distance from the point. Only a circular neighborhood is possible. The volume under the surface equals the population field value for the point, or 1 if NONE is specified. The density at each output raster cell is calculated by adding the values of all the kernel surfaces where they overlay the raster cell center. The kernel function is based on the quartic kernel function described in Silverman (1986, p. 76, equation 4.5).

The input data for the density map was naturally occurring rockfalls for the state of New Mexico. We chose to use a search radius of 3000 m and the geodesic method (relating to the shortest possible line between two points on a sphere), the latter because we are using a Transverse Mercator projection. Output values are densities in square kilometers, with an output cell size of 500x500 m.

3.2 Rockfall susceptibility map using slope-angle criteria

The second map we produced assumes the mapped rock fall points of Cardinali et al. (1990) are statistically representative samples of a much larger set. Excluding human-related rock falls (i.e., along highways, which number 200), the mapped points of naturally occurring rockfall total 3,689. Underlying slope-angle values within the proximity of these mapped points are tabulated, and from the mean, standard deviation, and 5th percentiles of their frequency distribution we establish slope-based bins that we reason are reliable proxies for rockfall susceptibility. An annotated photograph illustrating estimating susceptibility using slope-angle criteria is presented in Figure 3.1. The workflow of our method is summarized in Figure 3.2 and presented in detail in Appendix A. Input data and interim rasters used in the various steps to make the final map are archived in Appendices B and C. The main steps of the process sequentially involve: sampling slope values, establishing slope bins based on statistically defined slope-angle boundaries, populating these bins from a Digital Elevation Model, generalizing (downsampling) the data to 1:750,000 scale, and conducting a rough validation process using histograms.

We did not explicitly incorporate lithology in our analyses for three reasons. One, the only statewide map coverage of geology (NMBGMR, 2002) contains an average spatial error of 200 m, consistent with the 1:500,000 scale, but in many places is inaccurate by 500-1000 m. Compounded with the inaccuracy in the Cardinali et al. (1990) rockfall dataset, this can create unacceptably high inaccuracies in many areas that would be time-consuming to locate and correct. Two, rockfalls usually accumulate on steep slopes below rockfall-generating cliffs or ledges. So where the rockfalls lie do not equate to their source area. Given the inaccuracies in the Cardinali et al. (1990) rockfall dataset, an automated approach to determining the true rockfall source would be difficult (e.g., Figure 2.5). Three, if one assumes the geomorphic principle of dynamic equilibrium, which was proposed for desert landscapes like much of New Mexico (Gilbert, 1877), then slope angles are relatively time-independent and are a function of the rock type (plus climate-modulated weathering and erosional processes). In other words, the hard rocks that could serve as rockfall sources would likely exhibit steep slopes, at least in the areas of rockfall.

3.2.1 Sampling slope values

Conceptually, we want to obtain a representative sample of slopes associated with the "at-rest" rockfalls in the run-out zone. As explained above, it is commonly difficult to relate at-rest rockfalls to geologic source units because of the 0-600 m spatial inaccuracy of mapped rockfalls in Cardinali et al. (1990) as well as uncertainties of correlating at-rest boulders to uphill source areas. However, we reason that rockfall source area slopes would be higher than these "at-rest" sampled slopes. To account for the spatial error, we sampled slopes within a 300 m-radius window surrounding a given rockfall point (Figure 3.3). We chose 300 m because it is the median of the error range. The first sampling procedure took the average of slope values within this window. The second procedure took the maximum slope values within this window. Histograms were constructed of these distributions (Figure 3.4). Comparison of these histograms indicate that the average of the window resulted in the slope distribution being heavily skewed to lower slope values (Figure 3.4a). This is because most of New Mexico consists of relatively wide expanses of low-sloping terrain punctuated by relatively narrower steep slopes. Thus, spatial errors would tend to place a point in low-sloping terrain (Figure 3.3), and taking the average

about a 300 m circle would result in relatively low slopes. In contrast, taking the maximum slope within the 300 m-radius window results in a quasi-normal, Gaussian distribution approximately centered on a peak correlating with the mean (Figure 3.4b). We think it is reasonable to associate rockfalls with steeper slopes within the 300 m radius sampling circle, and the resulting quasi-normal, Gaussian distribution is a better choice for using means and standard deviations. Thus, we use the results from the sampling of maximum slope.

3.2.2 Designating slope-angle bins

From the distribution of the maximum-slope values (Figure 3.4b), we calculated the mean and standard deviation using EXCEL (Appendix A). The mean value is 29° and the standard deviation is 12°. We used the mean-less-one-standard deviation of 17° to define the lower slope-value boundary for "Likely susceptible," which seemed reasonable based on the two-decade field mapping experience of the lead author. It is the ≥17° slopes that contain source-generating escarpments or ledges, consistent with the observation that practically all escarpments mapped by Cardinali et al. (1990) fall in this slope range (Plate 2).

Based on the lead author's field experience, it also seemed reasonable to include a buffer around the lower end of the "Likely susceptible" areas that could also receive limited rockfall, especially given that large rock falls could bounce and roll for appreciable distances from ≥17° slopes on a variety of <17° terrains. This downslope buffer slope bin is included in the "Potentially susceptible" zone. In order to remove mesa tops, we only include 5-16° slopes in the Potentially susceptible zone. It is reasonable to have the lower slope values in the buffer zone be 5° because the uppermost reaches of bouldery alluvial fans flanking mountain fronts, that could potentially receive rockfall, are often somewhat steep (~5° or more). Also, narrow canyons within Likely susceptible areas, whose flat floors could receive rockfalls from adjoining steep slopes, are subsumed into the Likely susceptible category using our generalization ARC procedures (described below). To determine the buffer distance, we determined the distance away from Likely susceptible areas (those with ≥17° slopes) that included the 90th percentile of the mapped rockfalls of Cardinali et al. (1990), excluding outliers (which are defined as twice the interquartile distance). This distance corresponds to 470 m (Appendix A).

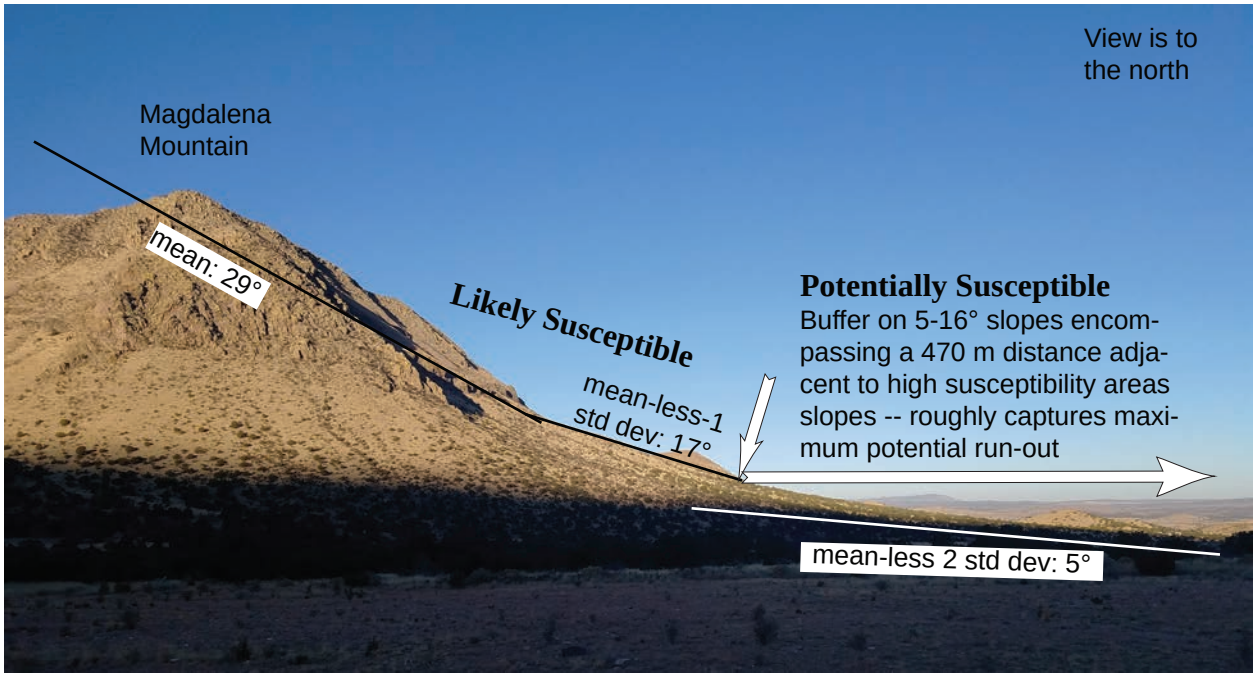

Figure 3.1. Illustration of slope-angle thresholds determined in this study. Magdalena Mountain serves as the photogenic backdrop. For all of New Mexico, the mean value of the maximum slopes surrounding Cardinali et al. (1990) mapped rockfall points (radius of 300 m) is 29°. Slopes corresponding to the mean-less-one standard deviation are categorized as Likely Susceptible. A buffer zone, restricted to 5-16° slopes, surrounds "Likely" susceptible areas and was designed to roughly capture the maximum potential run-out zone. The lower slope range of 5° corresponds to mean-less-two standard deviations, and 5° is approximately the lower slope found in the upper parts of bouldery alluvial fans. The "Potentially" susceptible category includes this buffer as well as all slopes with values of 8-16°. The "Unlikely" susceptible category includes <8° slopes outside of the buffer zone. Figure 3.5 further explains the rationale for using these slope values.

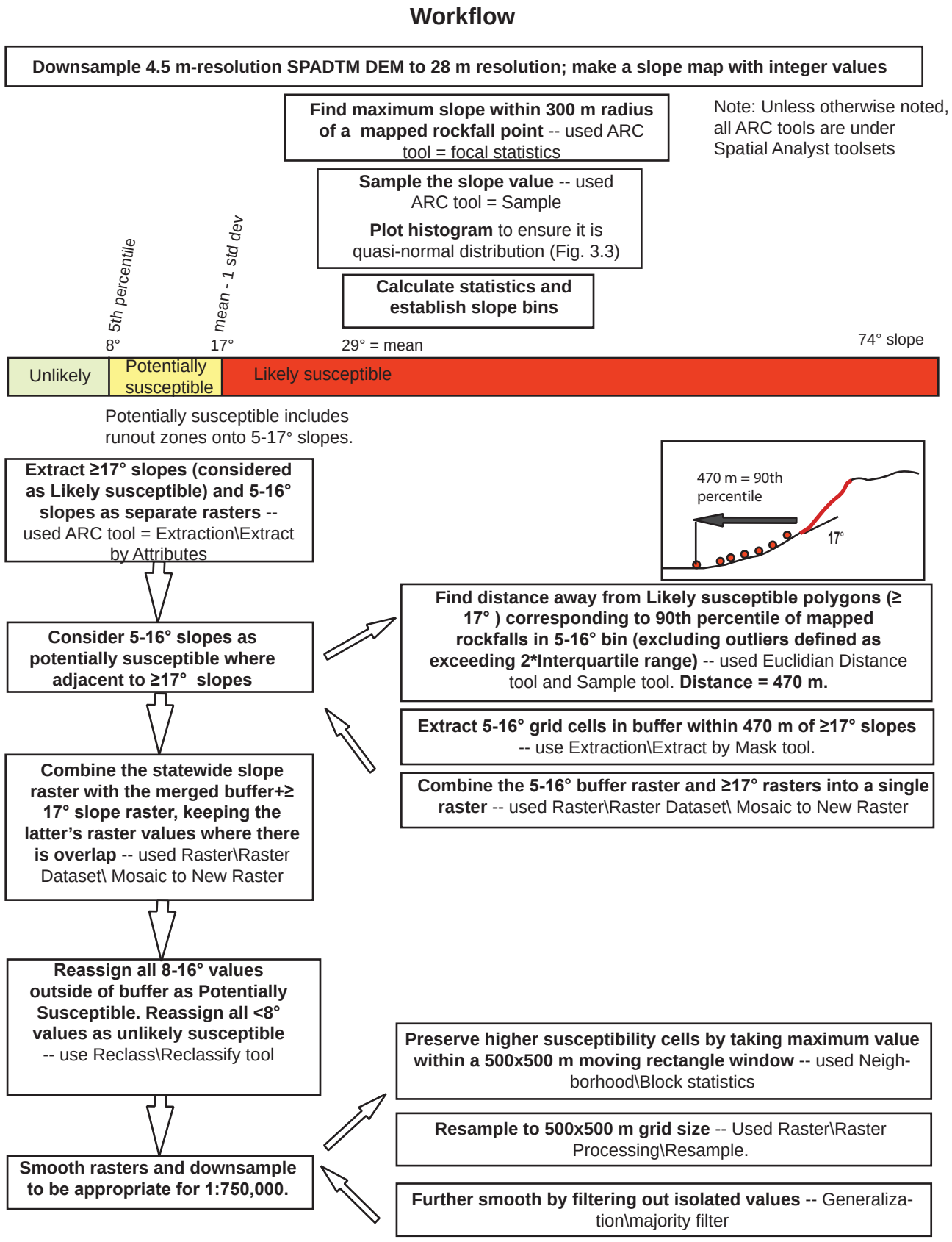

Figure 3.2. Illustration of the workflow to construct rockfall susceptibility maps using the slope-angle method.

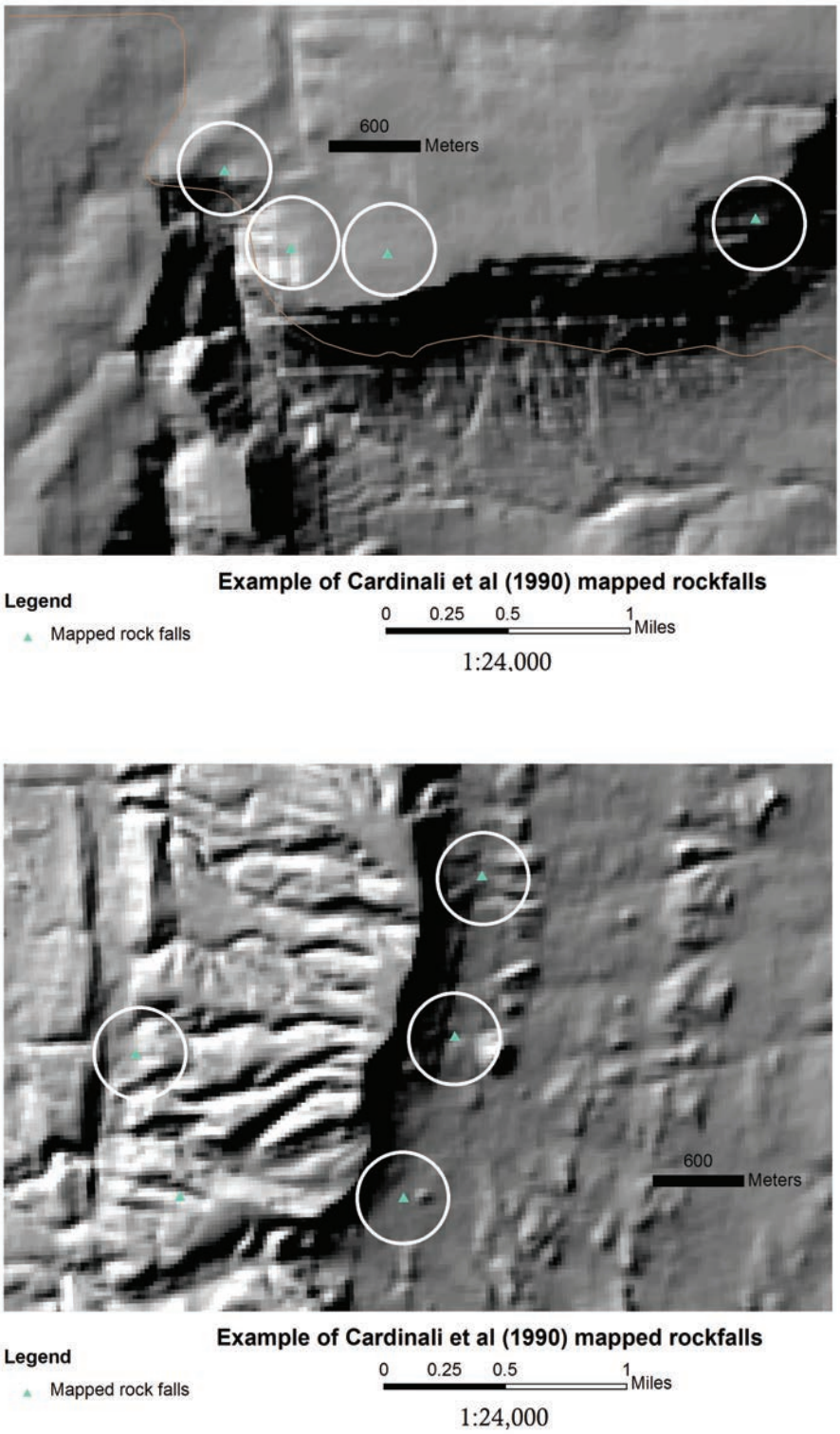

Figure 3.3. Examples of 300 m-radius error circles around mapped rockfall points of Cardinali et al. (1990). Taking an average of the error circles would result in an unrealistic relatively low slope value (Figure 3-2). However, taking the maximum slope within the error circles would better approximate where most rockfalls are located (i.e., on steep slopes).

Figure 3.4 (next page). Histogram of sampling slopes in the proximity of the natural rockfall points of Cardinali et al. (1990). A) Frequency distribution obtained from sampling the average of slopes within the 300 m-radius sampling window. Note the data is heavily skewed towards lower values. Given that most of New Mexico consists of relatively low-sloping expanses punctuated by sparser steeper slopes, spatial errors of 0-600 m would likely result in an error point being placed on low-sloping ground. Hence, averaging slope values within the 300 m-radius window would be expected to give relatively low values. B) Frequency distribution obtained from sampling the maximum slope within the 300 m-radius sampling window. Note the quasi normal (Gaussian) distribution, with the peak approximately centered on the mean value of 29 degrees.

A)

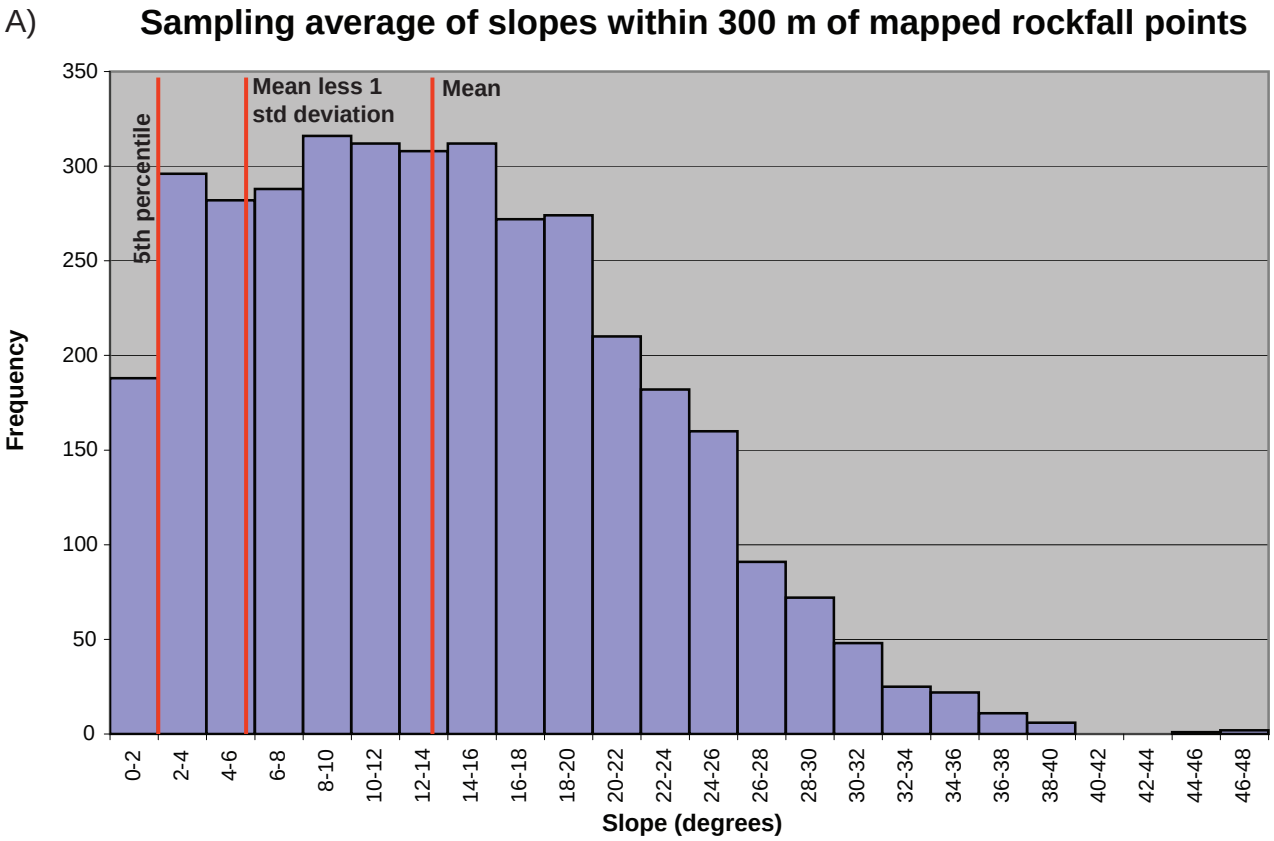
Sampling average of slopes within 300 m of mapped rockfall points
Mean less 1 std deviation
Mean
5th percentile
Frequency
Slope (degrees)
0
50
100
150
200
250
300
350
0-2
2-4
4-6
6-8
8-10
10-12
12-14
14-16
16-18
18-20
20-22
22-24
24-26
26-28
28-30
30-32
32-34
34-36
36-38
38-40
40-42
42-44
44-46
46-48

B)

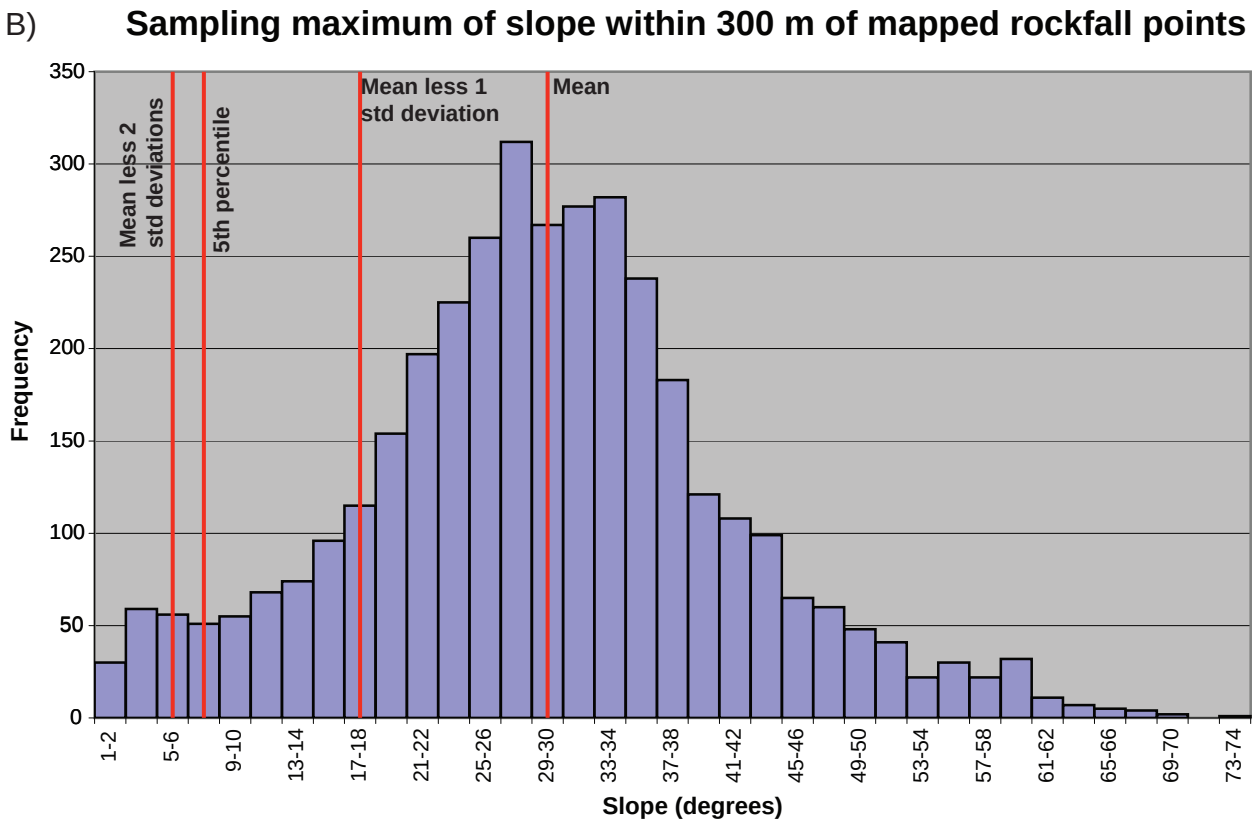
Sampling maximum of slope within 300 m of mapped rockfall points
Mean less 2 std deviations
5th percentile
Mean less 1 std deviation
Mean
Frequency
Slope (degrees)
0
50
100
150
200
250
300
350
1-2
5-6
9-10
13-14
17-18
21-22
25-26
29-30
33-34
37-38
41-42
45-46
49-50
53-54
57-58
61-62
65-66
69-70
73-74

Away from the buffer zone and high susceptibility areas, slope values <17° were classified as Potentially susceptible or Unlikely susceptible. The mean-less-5th percentile encompasses slopes in the 8-17° range. These moderately low sloping areas may receive rockfall from adjoining areas of ≥17° slopes, or they may contain small rockfall-generating ledges not captured on a 28 m DEM. (Figure 9). Thus, they were classified as Potentially susceptible along with the buffer zone slope values. Slopes <8° outside of the buffer zone are classified as "Unlikely susceptible" because they probably do not have noteworthy rockfall-generating ledges nor are they expected to lie in rockfall run-out zones. Illustrations of how slopes relate to the buffer zone, as well as our three susceptibility categories is given in Figures 3.1 and 3.5.

3.2.3 Workflow for populating slope bins

Once we established the slope-angle boundaries, we extracted slope bins using ARC procedures (Spatial Analyst Tools\Extraction\Extract by attributes). Also, we established a buffer zone around Likely susceptible areas and included it in the Potentially susceptible category. Our ARC procedure for establishing these bins is outlined in the table below.

Table 1. ARC-related procedures for establishing susceptibility bins after slope-angle boundaries are defined.

Procedure	**ARC tool**
Calculate slopes from a 28 m DEM	Spatial Analyst\Surface\Slope
Extract ≥17° slopes from 28 m DEM	Spatial Analyst Tools\Extraction\Extract by Attributes
Reassign all ≥17° slopes into a single numerical value corresponding to "Likely susceptible." Representative integer value chosen is 90.	Spatial Analyst Tools\Reclass\Reclassify
Extract 5-16° slopes from 28 m DEM	Spatial Analyst Tools\Extraction\Extract by Attributes
Reassign all the 5-16 degree values to a single value corresponding to "Potentially susceptible." Representative integer value chosen is 85.	Spatial Analyst Tools\Reclass\Reclassify
Within the 85 bin, determine which distance away from Likely susceptible areas (90 bin) corresponds with the 90th percentile of mapped rockfalls (excluding outliers that are defined as '2 times the interquartile distance'). Distance = 470 m.	Spatial Analyst Tools\Distance\Euclidian Distance Spatial Analyst Tools\Extraction\Sample
Find euclidian distance from Likely susceptible areas, using a maximum distance of 470 m.	Spatial Analyst\Distance\Euclidian Distance
Reclassify the distance of 0-470 m as a single value.	Spatial Analyst Tools\Reclass\Reclassify
Extract 5-16° data within 470 m of the ≥17°. This is the potential run-out buffer.	Spatial Analyst\ Extract\Extract by Mask Input was the Likely susceptible slopes (85

	value).
Combine the two rasters corresponding to the buffer and the Likely susceptible zones (≥17° slopes) into a new raster.	DataManagement\raster\mosaic to New Raster *Used mosaic operator of "sum." Defined 1 band.*
Combined this merged raster with the original slope raster (step #1). For overlapping pixels, assign the highest value. This preserves the pre-existing 85 (Potentially susceptible) and 90 (Likely susceptible) values.	DataManagement\raster\mosaic to New Raster *Used mosaic operator of "maximum" Defined 1 band.*
Reassign all the 0-16° values outside of the buffer to a one of two susceptibility classes: Potentially susceptible (8-16°) and Unlikely susceptible (<8°), respectively represented by integer values of 85 and 83.	Spatial Analyst\ Reclass\Reclassify
To preserve higher susceptible cells (conservative approach), take the maximum cell value within a 500x500 m moving window (rectangle-shaped)	Spatial Analyst\neighborhood\block statistics
Resample to 500x500 m grid size	Data Management\Raster\ RasterProcessing\Resample
Do a majority filter pass in order to subsume isolated grid values	Spatial Analyst\generalization\majority filter *Number of neighbors: 8* *Replacement threshold: half*

3.2.4 Generalizing data to 1:750,000 scale

The processing conducted so far was performed using grid sizes of 28x28 m. This makes for a smoothed map appropriate for high scales, but is too detailed for the final desired map scale of 1:750,000. It is only at this scale that a final map can be plotted on 36 inch-wide paper.

We took a conservative approach in generalizing the data because we did not want to loose high-susceptibility grid values in the downsampling process. Therefore, we first accentuated the areas of higher susceptibility (i.e., Likely susceptible category) by conducting a neighborhood block routine to capture the maximum value for a cell centered within a moving 500x500 m moving rectangle. Then, we resampled the raster to 500x500 m grid size. Finally, we conducted a majority filter over the data to subsume isolated grid values into the larger majority. The differences between the pre-generalized and generalized maps are illustrated in Figures 3.6.

3.2.5 Validation

In addition to qualitative, visual inspection of the final product, we conducted a simple verification technique. On the final map (Plate 2), we sampled the susceptibility bins under the mapped rock falls of Cardinali et al. (1990). The majority of these mapped rockfalls should fall into the "Likely susceptible" category Inspection of the associated histogram indicates that 85% of the mapped points fall in the "Likely susceptible" category and 12% fall in the "Potentially susceptible" category (Figure 3.7).

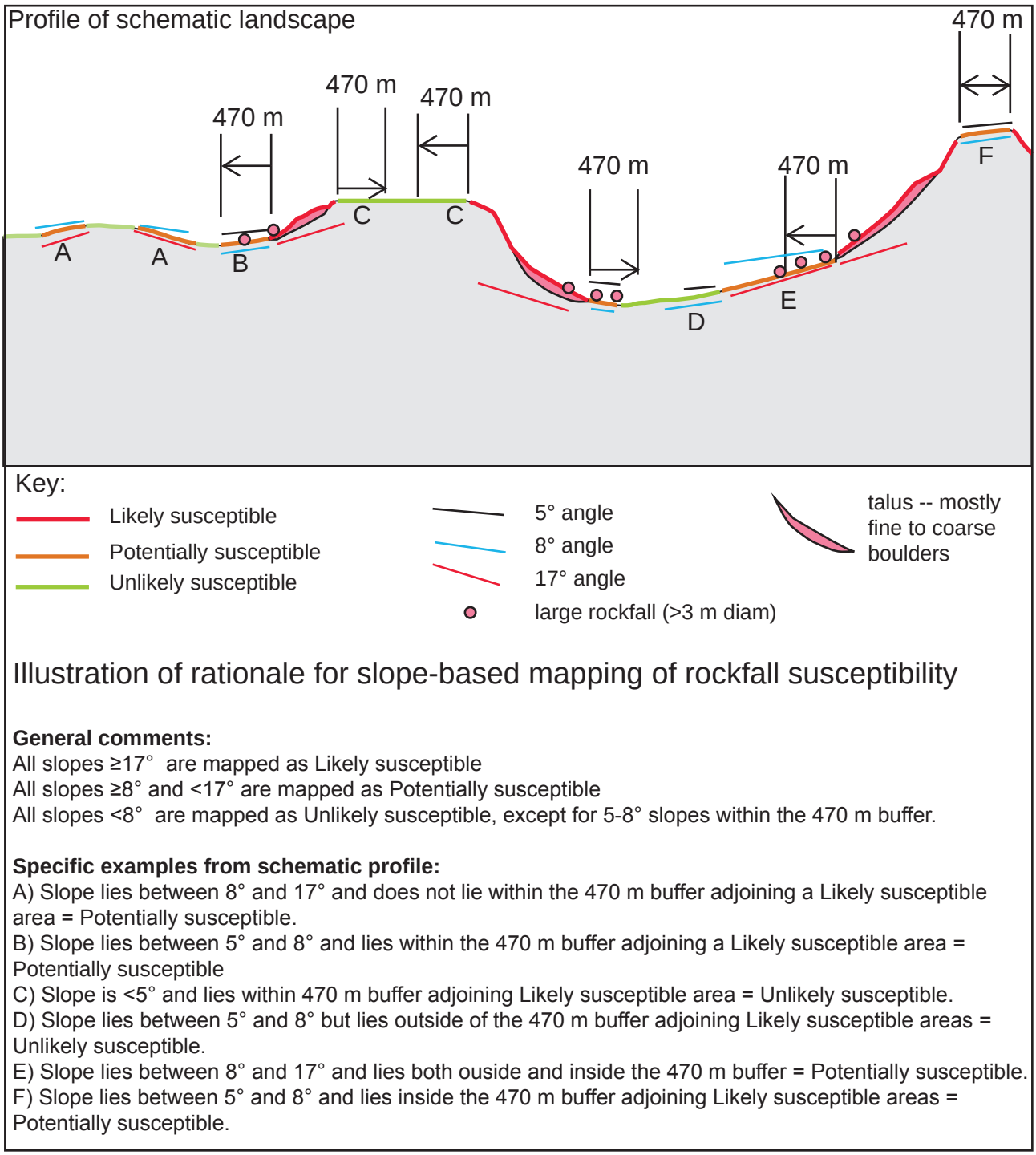

Illustration of rationale for slope-based mapping of rockfall susceptibility

General comments:
All slopes ≥17° are mapped as Likely susceptible
All slopes ≥8° and <17° are mapped as Potentially susceptible
All slopes <8° are mapped as Unlikely susceptible, except for 5-8° slopes within the 470 m buffer.

Specific examples from schematic profile:
A) Slope lies between 8° and 17° and does not lie within the 470 m buffer adjoining a Likely susceptible area = Potentially susceptible.
B) Slope lies between 5° and 8° and lies within the 470 m buffer adjoining a Likely susceptible area = Potentially susceptible
C) Slope is <5° and lies within 470 m buffer adjoining Likely susceptible area = Unlikely susceptible.
D) Slope lies between 5° and 8° but lies outside of the 470 m buffer adjoining Likely susceptible areas = Unlikely susceptible.
E) Slope lies between 8° and 17° and lies both ouside and inside the 470 m buffer = Potentially susceptible.
F) Slope lies between 5° and 8° and lies inside the 470 m buffer adjoining Likely susceptible areas = Potentially susceptible.

Figure 3.5. Illustration of the rationale used for slope-based mapping of rockfall susceptibility using an annotated profile of a schematic landscape.

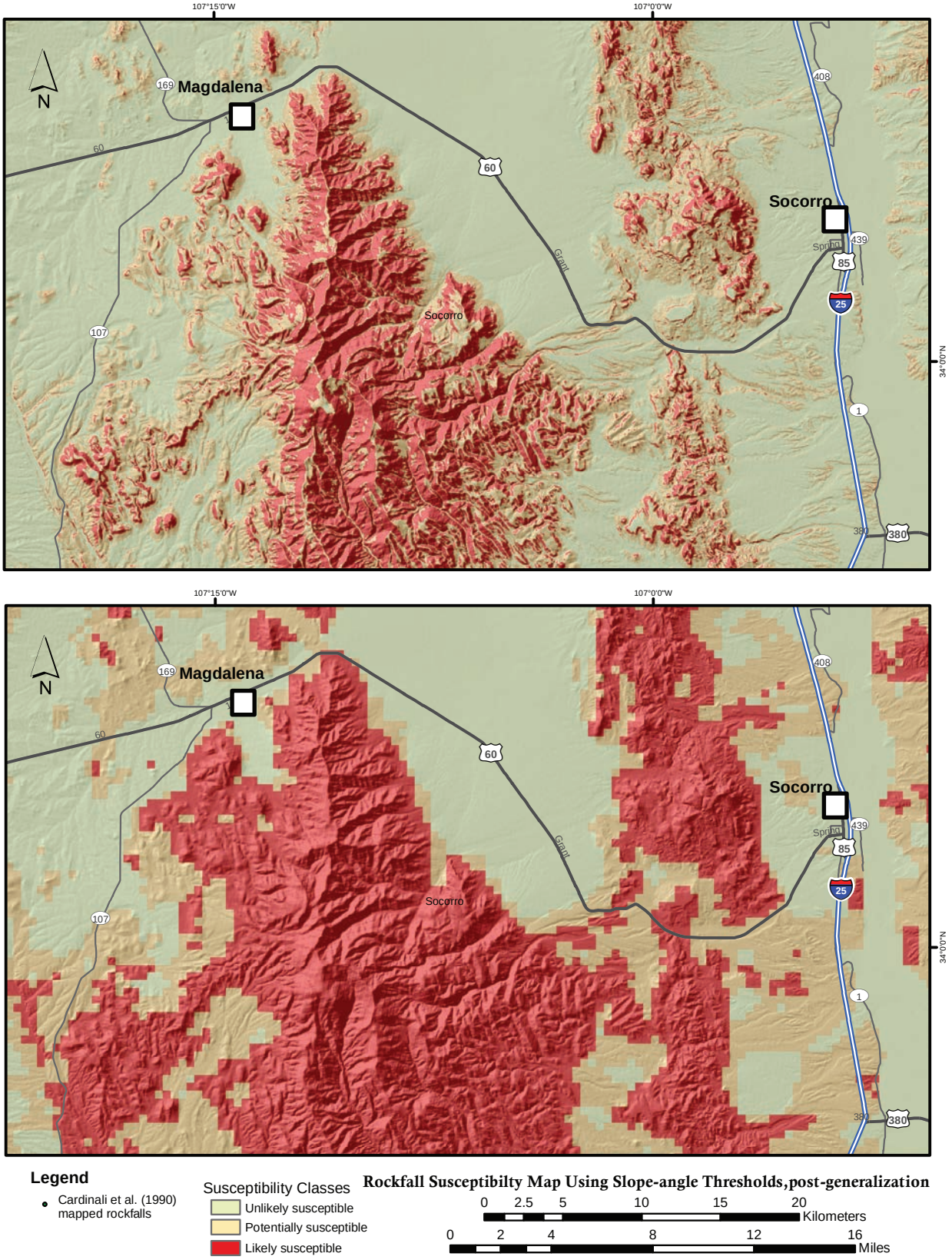

Figure 3.6. Illustration of pre-generalization (top) and post-generalization (bottom) rockfall susceptibility map constructed using slope-angle criteria. This was done to make the map consistent with the final 1:750,000. Note the scale shown here is roughly twice the scale of 1:750,000, and hence is more detailed than the final scale. Depicted area is near Socorro, NM.

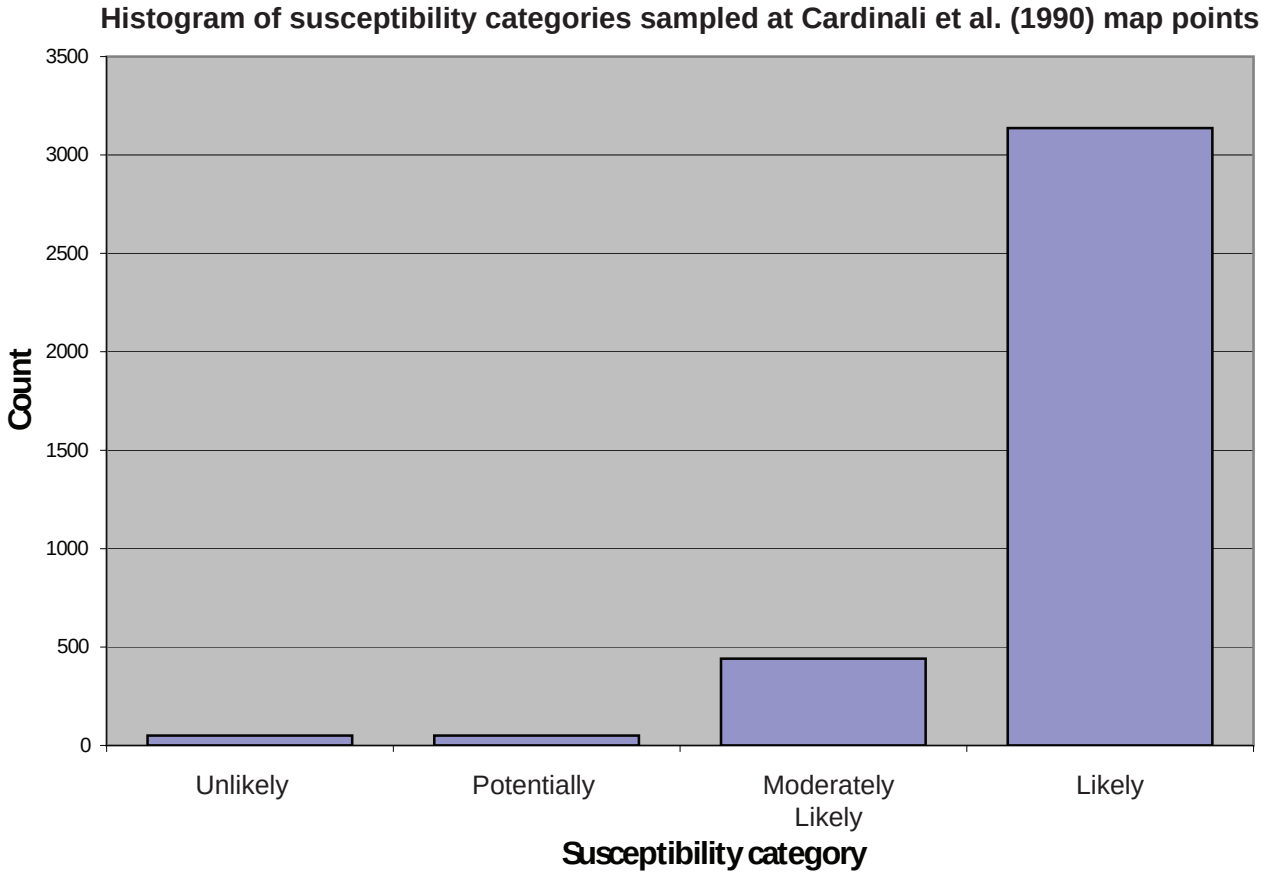

Figure 3.7. Histogram of verification sampling, where we sampled the rockfall susceptibility category using the "naturally occurring" rockfall points of Cardinali et al. (1990).

4 Results

The two types of rockfall susceptibility maps for the entire state are presented in Plates 1 and 2. Figures 4.1 and 4.2 depict page-size versions of these larger plots. A detailed view of the Albuquerque area is shown in Figure 4.3, which illustrates the differences of the two maps at a more detailed scale. The ARC GIS map packages associated with the final product are found in Appendix D.

In Plate 1 and Figure 1, high densities of rockfalls are shown in mountainous areas. However, there is a bias for rockfalls along major roads, even though only "naturally occurring" rockfalls were contoured. This may be due to errors in the original Cardinali et al. (1990) dataset. As mentioned in the Methods section, this map likely is biased towards large rockfalls that could be readily noted in aerial photographs.

Plate 2, generated by the slope-angle method detailed above, should capture a wider range of rockfall sizes because it is a function of slope steepness. Note that this method does not differentiate between susceptibility at the source and susceptibility in the run-out zone. Rather, the two are lumped together in terms of susceptibility. This map depicts a conservative view of where rockfall activity may occur in the state. As noted in the legend, Likely susceptible zones contain local areas (over approx. distances of 300-1000 m) with ledges or cliffs that could generate rockfalls, and slopes may be sufficiently steep to allow rockfall transport over various distances. In Potentially susceptible zones, slopes may possibly contain small ledges that could generate limited rockfall with short transport paths (probably less than 100 m). This susceptibility class also includes possible run-out zones, on slopes of 5-17°, that could extend up to ~470 m downslope from the base of $\geq$17° slopes, although most run-outs would be expected to be much shorter. Unlikely susceptible is designated for low slopes (<8°), except for 5-8° slopes in run-out zones (the buffer described in the methods section), and are considered unlikely for either generating or transporting rockfalls.

Visually, there is good correspondence of mountains and other steep-sloped areas with Likely susceptible zones. Vast amounts of the state are hilly with moderate slopes (8-17°). These areas are classified as Potentially susceptible, which may possibly contain small rockfall-producing ledges not captured by the input 28 m-resolution DEM. The moderate slopes in the "potentially susceptible" zones may potentially pose hazardous situations depending on anthrogenic activities. For example, these hilly terrains may be covered by a lag of gravel (of varying densities), and an artificial cut may create fall potential for these gravels (Figure 4.4). Note that comparing rockfall susceptibility areas with those pertaining to deep-seated landslide susceptibility (Cikoski and Koning, 2017) yield many areas of common overlap.

Figure 4.1 (next page). Page-size figure of Plate 1, which is best considered as a first-order approximation of susceptibility of large-block rockfalls. Preparedness areas relate to statewide emergency management (e.g., NMDHSEM, 2013).

Figure 4.2 (two pages). Page-size figure of Plate 2, which shows a rockfall susceptibility map of New Mexico using slope criteria. In our opinion, this is the better susceptibility map to address rockfall hazard because it probably encompasses a larger range of rockfall sizes. Preparedness areas relate to statewide emergency management (e.g., NMDHSEM, 2013).

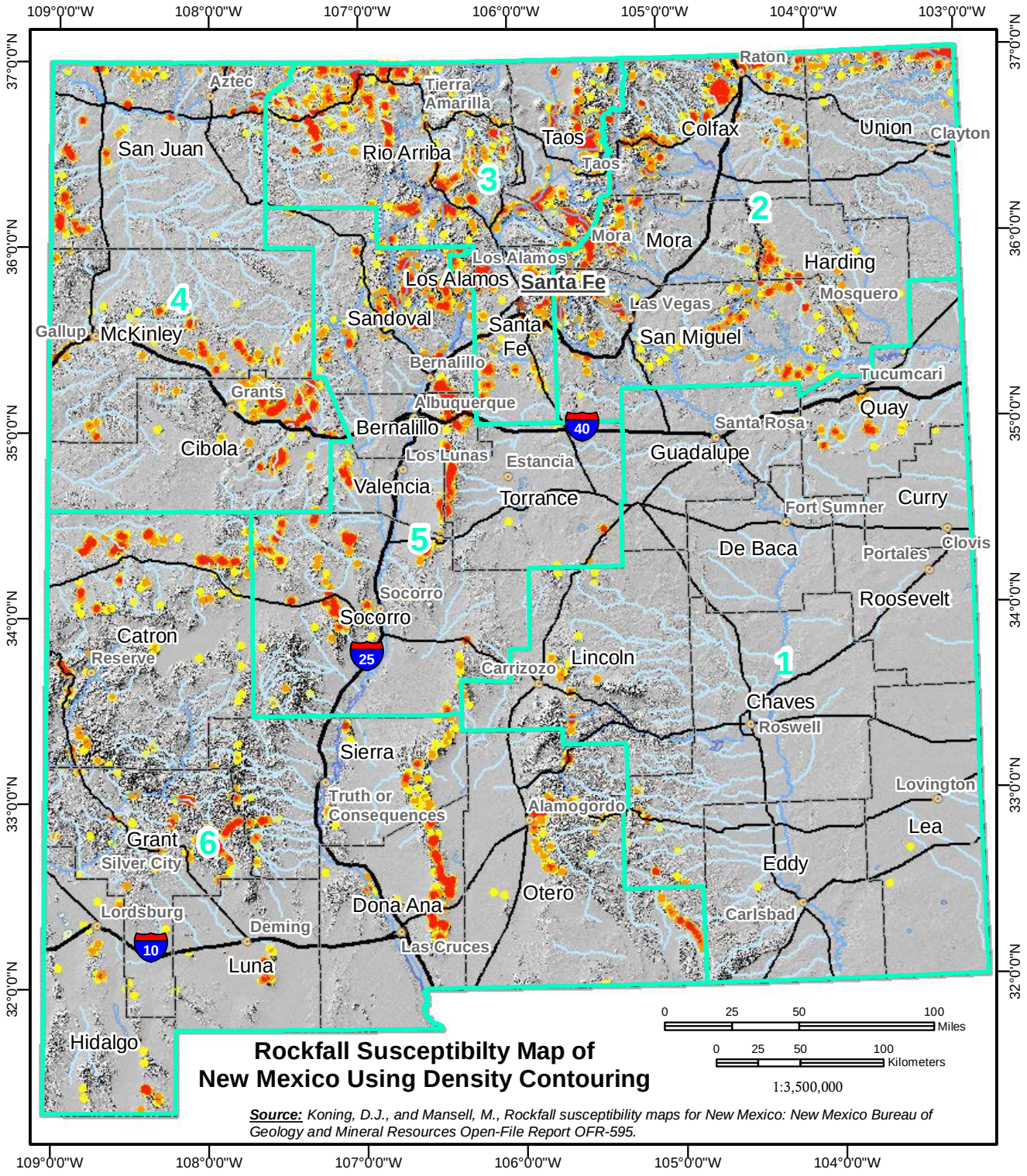

Rockfall Susceptibilty Map of New Mexico Using Density Contouring

Source: *Koning, D.J., and Mansell, M., Rockfall susceptibility maps for New Mexico: New Mexico Bureau of Geology and Mineral Resources Open-File Report OFR-595.*

Legend

Kernel density of rockfall points (search radius of 3 km), equal-frequency binned (in sq km)

- 0.01 - 0.035
- 0.035 - 0.070
- 0.070 - 0.14
- 0.14 - 0.64

1 Preparedness Area (labeled)

New Mexico Tech
SCIENCE · ENGINEERING · RESEARCH · UNIVERSITY

New Mexico Bureau of Geology and Mineral Resources
New Mexico Tech
Earth Science for the 21st Century

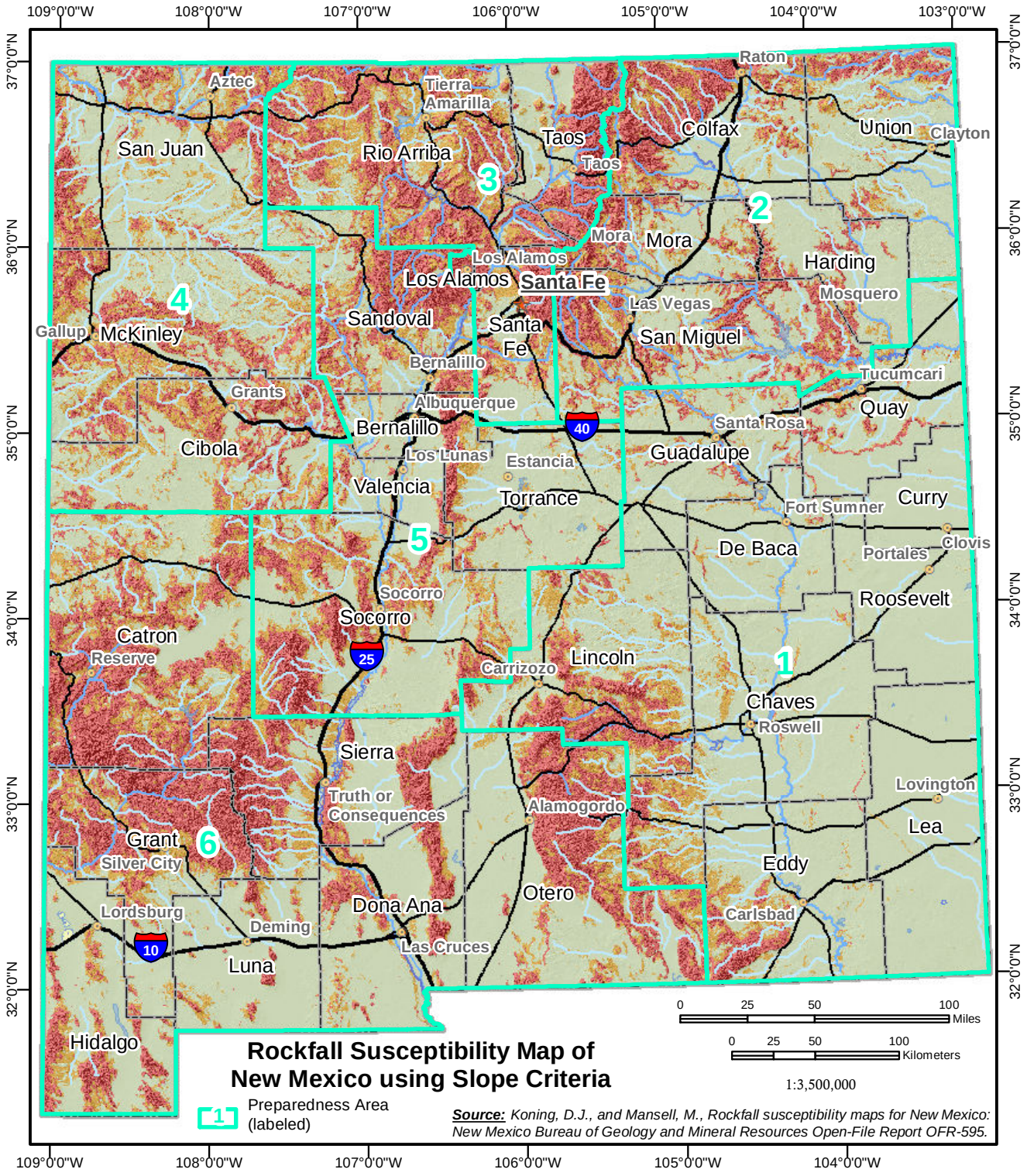

Unlikely Susceptible	Slopes that are <8° and considered unlikely for either generating or transporting rockfalls.
Potentially Susceptible	Slopes that are generally 8-17°. These slopes may possibly contain small ledges that could generate limited rockfall with short transport paths (<100 m). This susceptibility class also includes possible run-out zones (having slopes of 5-17°) that extend up to ~470 m downslope from the base of ≥17° slopes, although most run-outs will be much shorter.
Likely Susceptible	Slopes that are ≥17°, which correspond to the mean-less-one standard deviation of the maximum slopes within 300 m of mapped rockfalls (Cardinali et al., 1990). In this class are local areas (over approx. distances of 300-1000 m) containing ledges or cliffs that could generate rockfalls, and slopes may be sufficiently steep to allow rockfall transport.

Figure 4.3 (next page). Illustration of the spatial depiction of rockfall hazard for the ABQ area. Top: Map showing the point-density contouring of mapped rockfalls (from Plate 1). This map may serve as a proxy for where larger rockfalls may be expected to occur, based on past mapping from aerial photography (Cardinali et al., 1990). Density is mapped rockfalls per square kilometer. Bottom: A slope-based rockfall susceptibility map (from Plate 2). This map depicts a relatively conservative view of the hazard posed by a wider range of rockfall sizes.

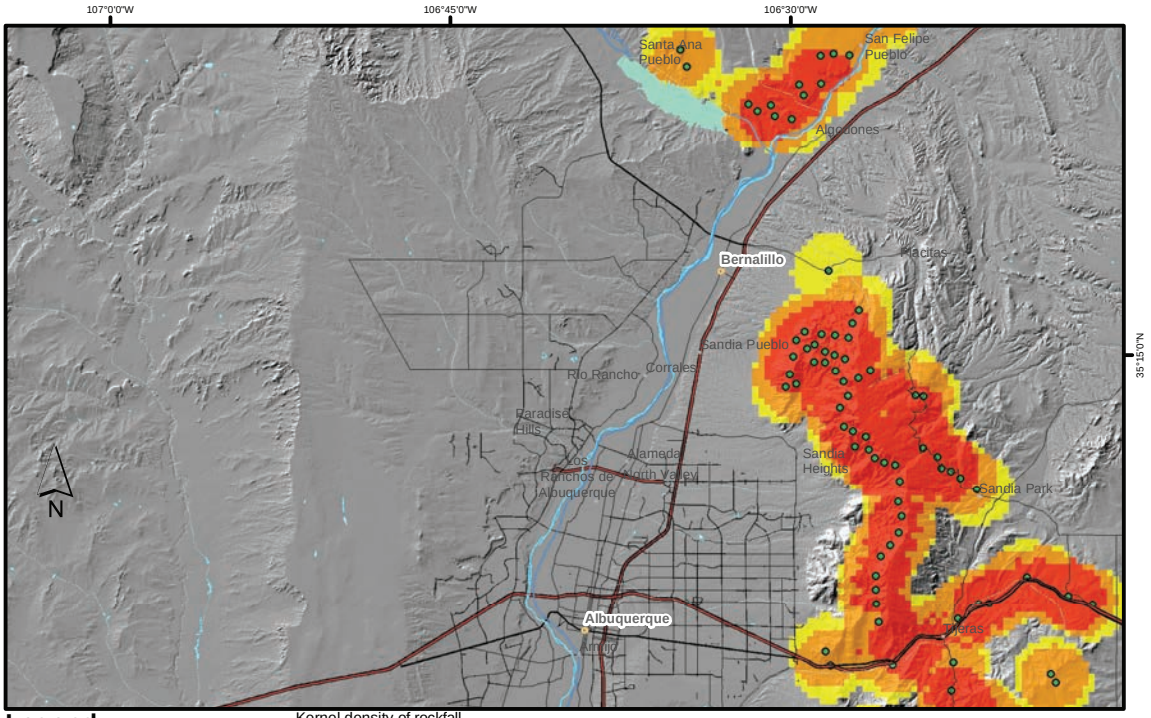

Legend

- Interstate
- US & State Highways
- Other road
- Naturally occurring rockfalls

Kernel density of rockfall points (search radiuus of 3 km), equal-frequency binned (in sq km)

- 0.01 - 0.035
- 0.035 - 0.070
- 0.070 - 0.14
- 0.14 - 0.64

Rockfall Hazard Map using Density Contouring

0 2.5 5 10 15 20 Kilometers

0 2.5 5 10 15 20 Miles

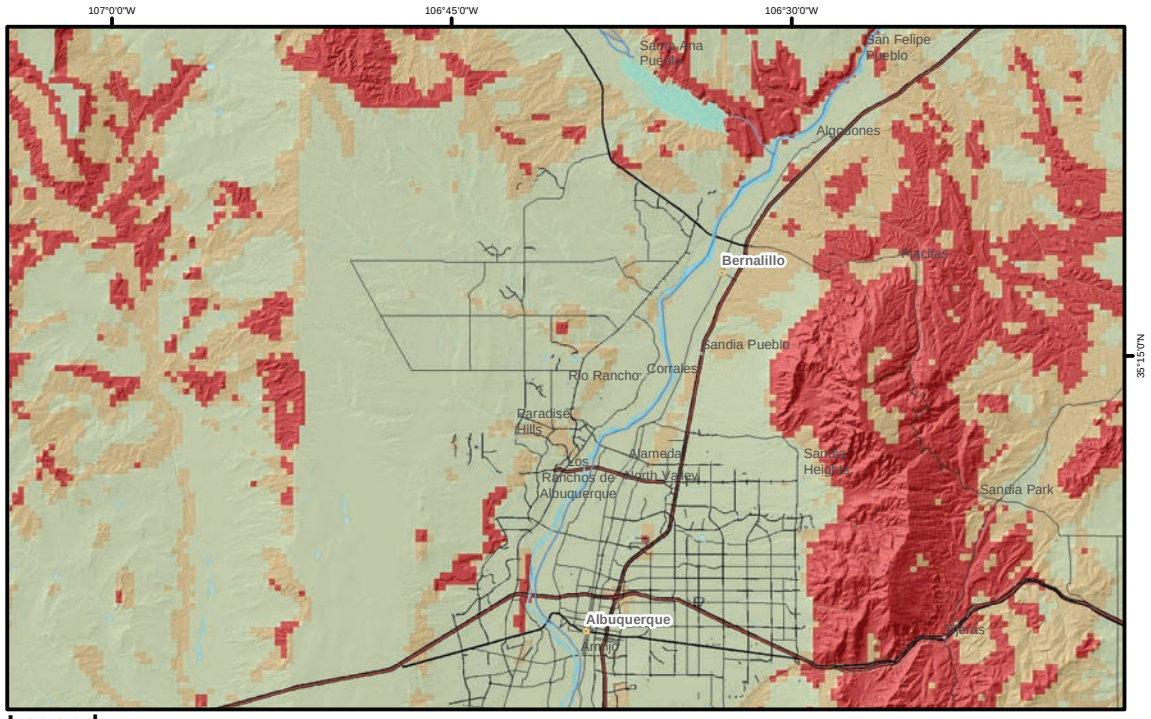

Legend

- Interstate
- US & State Highways
- Other road

Susceptibility Classes

- Unlikely susceptible
- Potentially susceptible
- Likely susceptible

Rockfall Susceptibilty Map Using Slope-angle Criteria

0 2.5 5 10 15 20 Kilometers

0 2.5 5 10 15 20 Miles

N

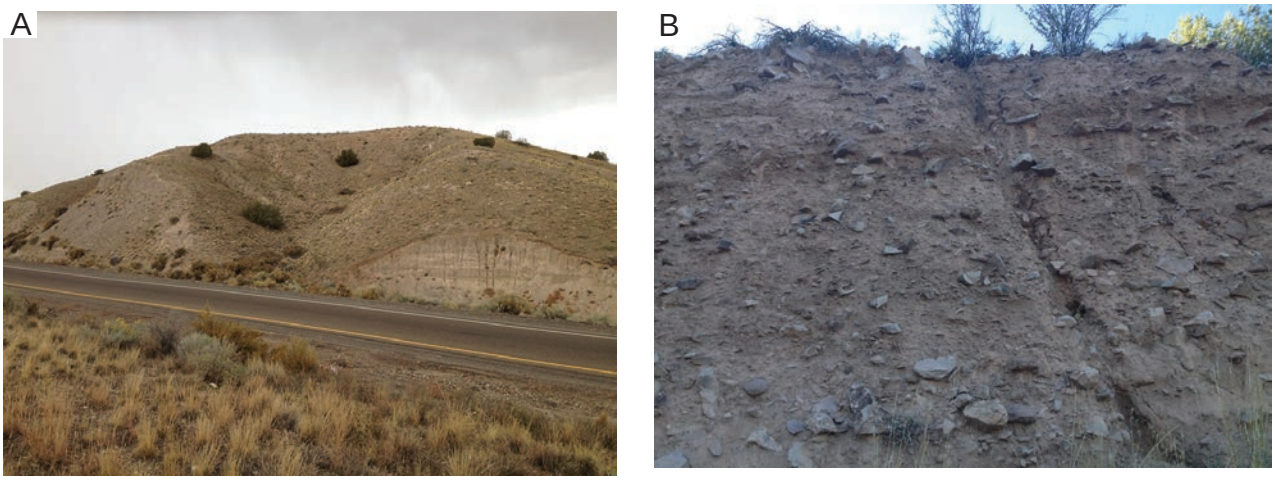

Figure 4.4. Photographs illustrating terrain that may be captured by the Potentially susceptible category. A) Photo of hills 6.7 km northeast of the town of Algodones. Gravels that mantle hillslopes such as these could roll short distances down 5-17° slopes, especially where artificial cuts are created by human activity. B) Photo of a roadcut along U.S. Highway between the towns of Reserve and Alma. If a cut-bank involves gravelly material, like shown here, clasts could fall off the steep slope and roll onto the road. Potentially susceptible areas shown in Plate 2 may spatially coincide with gravelly sediment, which often underlies hilly surfaces with 5-17° slopes.

5 Discussion

5.1 Use of maps and associated limitations

The resulting rockfall susceptibility maps (Plates 1 and 2) should be a useful planning tool for regional endeavors related to public safety, regional land use planning, and construction projects involving long distances. Examples of study sizes suitable for using this map (at a scale 1:750,000 and with a raster pixel resolution of 500 m) include the entire state, counties, the larger Indian reservations, or large municipalities (e.g., Albuquerque, Santa Fe, Las Cruces). The final map indicates areas where rockfall potential is not negligible and where reasonable probabilities may exist for rockfall. Given the broad-brush methodology and low-scale of these maps, they are not a substitute for a site-specific geologic or geotechnical study.

Limitations mainly involve issues of scale and risk assessment. The map should not be utilized for projects involving relatively small areas (<10 km^2), except to alert planners where a site-specific study may be warranted. Furthermore, this map does not convey information regarding frequency of occurrence or rockfall intensity (magnitude). Interpretations regarding frequency would require detailed mapping of individual rockfalls over an appreciable area in addition to age control for individual rockfall events. Estimating rockfall intensity would require a statewide modeling effort of expected rockfall kinetic energy or momentum, which would be a formidable task. This map also does not contain information pertaining to societal costs (including human injury or death) that might arise in a future rockfall event. Below, we list specific topics for which our rockfall maps may find application.

5.1.1 Public safety

The lack of rockfall frequency and intensity (kinetic energy) data inhibits these maps being used directly for risk assessment. However, these maps could be used to spatially compare relative rockfall hazard in different parts of the state. For example, New Mexico has been subdivided into Preparedness Areas for the purposes of emergency planning (NMDHSEM, 2013), as shown on Figures 4.1-4.2. The rockfall density data (Fig. 4.1) and slope-based susceptibility data (Fig. 4.2) could be used to compare the relative differences in rockfall hazards between Preparedness Areas. Consequently, this susceptibility map would have notable value in updating the Hazard Identification/Risk Assessment Section and Vulnerabilities Section in the New Mexico State Hazard Mitigation Plan.

5.1.2 Regional land use planning

The maps in Plates 1-2 could play a role in regional land use studies. For future residential or commercial development, for example, regional zoning maps (e.g., county level) could stipulate that detailed site studies be conducted in areas of Likely susceptibility. Road planning associated with these development may need to include mitigation measures to reduce rockfall hazards.

Our rockfall susceptibility map could be an asset in the planning of long-distance transportation or utility corridors across New Mexico. Specifically, this map could be used to identify large regions that are Likely susceptible to rockfall, which could be avoided in various

planning scenarios. If a Likely susceptible area must be crossed by the corridor, then a site-specific study employing an engineering geologist would be warranted. It could also alert the NM Department of Transportation to areas that may require more road maintenance.

5.1.3 Construction projects

Most construction projects involve areas less than <10 km^2, and so this susceptibility map would not be useful except for alerting planners where a site-specific study should be conducted. However, this map would be useful in long-distance construction projects, as explained in the preceding sub-section. In addition to site-specific studies, extra vigilance may be warranted in Potentially susceptible or Likely susceptible zones. For example, creating artificial cuts in areas classified as Potentially susceptible or Likely susceptible could create local rockfall hazard potential due to fall surficial gravel.

6 References

Acosta, E., Agliardi, F., Crosta, G.B., and Rios Aragues, S., 2003, Regional rockfall hazard assessment in the Benasque Valley (central Pyrenees) using a 3D numerical approach: Proceedings of the 4th EGS Plinius Conference held at Mallorca, Spain, October 2002.

Adams, J., 1980, Contemporary uplift and erosion of the Southern Alps, New Zealand: Geological Society of America Bulletin, v. 91, p. 1-114.

Akagawa, S., and Fukuda, M., 1991, Frost heave mechanism in welded tuff: Permafrost and Periglacial Processes, v. 2, no. 4, p. 301-309.

Aleotti, P., and Chowdhury, R., 1999, Landslide hazard assessment: summary review and new perspectives: Bulletin of Engineering Geology and the Environment, v. 48, p. 21-44.

Amit, R., Gerson, R., and Yaalon, D.H., 1993, Stages and rate of the gravel shattering process by salts in desert Reg soils: Geoderma, v. 57, p. 295-324, doi 10.1016/0016-7061(93)90011-9.

Anderson, R.S., 1998, Near-surface thermal profiles in alpine bedrock: implications for the frost weathering of rock: Arctic and Alpine Research, v. 30, no. 4, p. 362-372.

Antoniuou, A.A., and Lekkas, E., 2010, Rockfall susceptibility map for Athinios port, Santorini Island, Greece: Geomorphology, v. 118, p. 152-166.

Bathrellos, G.D., Skilodimou, H.D., and Maraoukian, J., 2014, The spatial distribution of middle and late Pleistocene cirques in Greece: Environmental Earth Sciences, v. 96, p. 323-338. doi: 10.1111/geoa.12044.

Berti, M., Genevois, R., Simoni, A., and Tecca, P.R., 1999, Field observation of a debris flow event in the Dolomites: Geomorphology, v. 29, p. 265-274.

Bloom, A.L., 1998, Geomorphology—A Systematic Analysis of Late Cenozoic Landforms, 3rd Edition: New Jersey, Prentice Hall, 482 p.

Boeckli, L., Brenning, A., Gruber, S., and Noetzli, J., 2011, A statistical permafrost distribution model for the European Alps: Cryosphere Discussions, v. 5, issue. 3, p. 1419-1459. doi: 10.5194/tcd-5-1419-2011.

Boelhouwers, J., and Jonnson, M., 2013, Critical assessment of the 2 °C min^{-1} threshold for thermal stress weathering: Geografiska Annaler, ser A, Physical Geography, v. 95, no. 4, p. 285-293, doi: 10.11111/geoa.12026.

Brabb, E.E., 1984, Innovative approaches to landslide hazard mapping: Proceedings of the 4th International Symposium on Landslides, Toronto, vol. 1, p. 307-324.

Budetta, P., and Nappi, M., 2013, Comparison between qualitative rockfall risk rating systems for a road affected by high traffic intensity: Natural Hazards and Earth Systems Sciences, v. 13, issue 6, p. 1643-1653.

Cardinali, M., Guzzetti, F., and Brabb, E.E., 1990, Preliminary maps showing landslide deposits and related features in New Mexico: U.S. Geological Survey, Open-file Report 90-293, scale 1:500,000.

Church, M., Stock, R.F., and Ryder, J.M., 1979, Contemporary sedimentary environments on Baffin Island, N.W.T., Canada: Debris slope accumulations: Arctic and Alpine Research, v. 11, no. 4, p. 371-402.

Cikoski, C.T., and Koning, D.J., 2017, Deep-seated landslide susceptibility map of New Mexico: New Mexico Bureau of Geology and Mineral Resources Open-File Report OFR-594, 84 p., 1 plate, 9 digital appendices.

Collins, B.D., and Stock, G.M., 2016, Rockfall triggering by cyclic thermal stressing of exfoliation fractures: Nature Geoscience, v. 9, p. 395-401, doi 10.1038/NGEO2686.

Corò, D., Galgaro, A., Fontana, A., and Carton, A., 2015, A regional rockfall database: the Eastern Alps test site: Environmental and Earth Sciences, v. 74, p. 1731-1742.

Coutard, J.P., and Francou, B., 1989, Rock temperature measurements in two alpine environments: implications for frost shattering: Arctic and Alpine Research, v. 21, no. 4, p. 399-416.

Cruden, D.M., and Varnes, D.J., 1996, Landslide types and processes, in Turner, A.K., and Schuster, R.L., eds., Landslides--Investigation and mitigation: Transportation Research Board, Special Report no. 247, National Research Council, National Academy Press, Washington, D.C., p. 36-75.

Davidson, G.P., and Nye, J.F., 1985, A photoelastic study of ice pressure in rock cracks: Cold Regions Science and Technology, v. 11, p. 143-153.

Dragovich, D., 1993, Fire-accelerated boulder weathering in the Pilbara, Western Australia: Zietschrift fur Geomörphologie, v. 37, p. 295-307.

Dorn, R.I., 2011, Revisiting dirt cracking as a physical weathering process in warm deserts: Geomorphology, v. 135, p. 129-142.

Eppes, M.C., Magi, B., Hallet, B., Delmelle, E., Mackenzie-Helnwein, P., Warren, K., and Swami, S., 2016, Deciphering the role of solar-induced thermal stresses in rock weathering: Geological Society of America Bulletin, v. 128, no. 9/10, p. 1315-1338.

Eppes, M.C., and Keanini, R., 2017, Mechanical weathering and rock erosion by climate-dependent subcritical cracking: Reviews of Geophysicis, v. 55, p. 470-508, doi: 10.1002/2017RG000557.

Fernandez-Hernández, M., Paredes, C., Castedo, R., Llorente, M., and Rogelio de la Vega-Panizo, 2011, Rockfall detachment susceptibility map in El Hierro Island, Canary Islands, Spain: Natural Hazards, v. 64, p. 1247-1271.

Ferrari, F., Giacomini, A., and Thoeni, K., 2016, Qualitative rockfall hazard assessment: A comprehensive review of current practices: Rock Mechanics and Rock Engineering, v. 49, p. 2865-2922.

Fischer, L., Kaab, A., Huggel, C., and Noetzli, J., 2006, Geology, glacier retreat, and permafrost degradation as controlling factors of slope instabilities in a high-mountain rock wall: the Monte Rosa east face: Natural Hazards and Earth System Sciences, v. 6, no. 5, p. 761-772. doi: 10.5194/nhess-6-761-2006.

Fischer, L., Purves, R.S., Huggel, C., Noetzly, J., and Haeberli, W., 2012, On the influence of topographic, geological, and cryospheric factors on the rock avalanches and rockfalls in high-mountain areas: Natural Hazards and Earth System Sciences, v. 12, no. 1, p. 241-254.

Frattini, P., Crosta, G., Carrara, A., and Agliardi, F., 2008, Assessment of rockfall susceptibility by integrating statistical and physically-based approaches: Geomorphology, v. 94, p. 419-437.

French, H.M., 1998, The Periglacial Environment, 2nd edition: Essex, Longman, 341 p.

Fryxell, F.M., and Horberg, L., 1943, Alpine mudflows at the Grand Teton National Park, Wyoming: Bulletin of the Geological Society of American, v. 54, p. 457-572.

Gilbert, G.K., 1877, Geology of the Henry Mountains (Utah) [U.S. Geographical and Geological Survey of the Rocky Mountain Region]: Washington, D.C., U.S. Government Printing office, 160 p. and 5 plates.

Giraud, R.E., and Shaw, L.M., 2007, Landslide susceptibility map of Utah: Utah Geological Survey Map 228DM, scale 1:500,000.

Gökçeoglu, C., and Aksoy, H., 1996, Landslide susceptibility mapping of the slopes in the residual soils of the Mengen region (Turkey) by deterministic stability analyses and image processing techniques: Engineering Geology, v. 44, p. 147-161.

Gouide, A.S., 2013, Arid and semi-arid geomorphology: Cambridge, UK: Cambridge University Press, 461 p., doi:10.1017/CB09780511794261.

Griggs, D.T., 1936, The factor of fatigue in rock exfoliation: The Journal of Geology, v. 44, no. 7, p. 783-796, doi:10.1086/624483.

Grossi, C., Brimblecombe, P., Menéndez, B., Benavente, D., Harris, I., and Déqué, M., 2011, Climatology of salt transitions and implications for stone weathering: The Science of the Total Environment, v. 409, no. 13, p. 2577-2585, doi 10.1016/j.scitoenv.2011.03.029.

Gudmundsson, A., 2011, Rock Fractures in Geological Processes: Cambridge, Cambridge University Press, 578 p.

Hales, T.C., and Roering, J.J., 2005, Climate-controlled variations in scree production, Southern Alps, New Zealand: Geology, v. 33, no. 9, p. 701-704.

Hales, T.C., and Roering, Joshua J., 2007, Climatic controls on frost cracking and implications for the evolution of bedrock landscapes: Journal of Geophysical Research, v. 112, F02033, 14 p. doi: 10.1029/2006JF000616.

Hallet, B., Walder, J., and Stubbs, C.W., 1991, Weathering by segregation ice growth in microcracks at sustained sub-zero temperatures: verification from an experimental study using acoustic emissions: Permafrost and Periglacial Processes, v. 2, p. 283-300.

Hall, K., and Thorn, C.E., 2014, Thermal fatigue and thermal shock in bedrock: An attempt to unravel the geomorphic processes and products: Geomorphology, v. 206, p. 1-13, doi: 10.1016/j.geomorph.2013.09.022.

Haneberg, W.C., and Bauer, P.W., 1993, Geologic setting and dynamics of a rockslide along NM 68, Rio Grande gorge, northern New Mexico: Bulletin of the Association of Engineering Geologists, v. 30, p. 7-16.

Haneberg, W.C., Bauer, P.W., and Chavez, W.X., Jr., 1992, Rio Grande Gorge Highway Corridor Study, Rinconada to Pilar: New Mexico Bureau of Mines and Mineral Resources Open-File Report 437, http:// http://geoinfo.nmt.edu/publications/openfile/details.cfml?Volume=437, last accessed Oct 24, 2017.

Herwig Proske, M., and Bauer, C., 2016, Rockfall susceptibility maps in Styria considering the protective effect of forest: Interpraevent 2016 -- Conference Proceedings, p. 592-600.

Highland, L.M., and Bobrowsky, P., 2008, The landslide handbook--A guide to understanding landslides: Reston, Virginia, U.S. Geological Survey Circular 1325, 129 p.

Hoek, E., 2007, Analysis of rockfall hazards, Chapter 9 *in* Practical Rock Engineering (self-published E-book), 25 p.

Hutchinson, J.N., 1995, Keynote paper: landslide hazard assessment: International Symposium on Landslides. Christchurch 3, p. 1805-1841.

Jiménez-Perálvarez, J.D., Irigaray, C., El Hamdouni, R., and Chacón, J., 2009, Building models for automatic landslide-susceptibility analysis, mapping and validation in ArcGIS: Natural Hazards, v. 50, no. 3, p. 571-590.

Jiménez-Perálvarez, J.D., Irigaray, C., El Hamdouni, R., and Chacón, J., 2011, Landslide-susceptibility mapping in a semi-arid mountain environment: an example from the southern slopes of Sierra Nevada (Granada, Spain): Bulletin of Engineering Geology and the Environment, v. 70, p. 265-277.

Krautblatter, M., and Moser, M., 2009, A nonlinear model coupling rockfall and rainfall intensity based on a four year measurement in a high Alpine rock wall (Reitnal, German Alps): Natural Hazards and Earth System Sciences, v. 9, p. 1425-1432.

Krautblatter, M., Huggel, C., Deline, P., and Hasler, A., 2012, Research perspectives on unstable high-alpine bedrock permafrost: measurement, modeling and process understanding: Permafrost and Periglacial Processes, v. 23, Issue 1, p. 80-88.

Loye, A., Jaboyedoff, M., and Pedrazzini, A., 2009, Identification of potential rockfall source areas at a regional scale using a DEM-based geomorphometric analysis: Natural Hazards and Earth Systems Science, v. 9, p. 1643-1653.

Luckman, B.H., 1976, Rockfalls and rockfall inventory data; some observations from the Surprise Valley, Jasper National Park, Canada: Earth Surface Processes and Landforms, v. 1, issue 3, p. 287-298.

Macciotta, R., Martin, C.D., Edwards, T., Cruden, D.M., and Keegan, T., 2015, Quantifying weather conditions for rock fall hazard management: Georisk, v. 9, issue 3, p. 171-186.

Marquínez, J., Menéndez Duarte, R., Farias, P., Jiménez Sanchez, M., 2003, Predictive GIS-based model of rockfall activity in mountain cliffs: Natural Hazards, v. 30, issue 3, p. 341-360.

Matsuoka, N., 2001, Direct observation of frost wedging in alpine bedrock: Earth Surface Processes and Landforms, v. 26, p. 601-614.

Matsuoka, N., and Sakai, H., 1999, Rockfall activity from an alpine cliff during thawing periods: Geomorphology, v. 28, no. 304, p. 309-328.

McFadden, L.D., Eppes, M.C., Gillespie, A.R., and Hallet, B., 2005, Physical weathering in arid landscapes due to diurnal variation in the direction of solar heating: Geological Society of America Bulletin, v. 117, no. 1/2, p. 161-173, doi: 10.1130/B25508.1.

Miller, D.J., and Dunne, T., 1996, Topographic perturbations of regional stresses and consequent bedrock fracturing: Journal of Geophysical Research, v. 101, p. 25,523-25,536, doi:10.1029/96JB02531.

Moores, J.E., Pelletier, J.D., and Smith, P.H., 2008, Crack propagation by differential insolation on desert surface clasts: Geomorphology, v. 102, p. 472-481.

Moreiras, S.M., 2005, Landslide incidence zonation in the Rio Mendoza valley, Mendoza Province, Argentina: Earth Surface Processes and Landforms, v. 29, p. 255-266.

Nagarajan, R., Roy, A., Vinod Kimur R., Mukherjee, A., and Khire, M.V., 2000, Landslide hazard susceptibility mapping based on terrain and climatic factors for tropical monsoon regions: Bulletin of Engineering Geology and the Environment, v. 58, p. 275-287.

NMDHSEM (New Mexico Department of Homeland Security and Emergency Management), 2013, New Mexico State Hazard Mitigation Plan: unpublished report by the New Mexico Department of Homeland Security and Emergency Management, 620 p. << http://www.nmdhsem.org/Mitigation.aspx, last accessed Nov. 3, 2017>>

NMBGMR (New Mexico Bureau of Geology and Mineral Resources), 2003, Geologic Map of New Mexico: New Mexico Bureau of Geology and Mineral Resources, scale 1:500,000.

Pachauri, A.K., and Pant, M., 1992, Landslide hazard mapping based on geological attributes: Engineering Geology, v. 32, p. 81-100.

Rapp, A., 1960, Talus slopes and mountain walls at Tempelfjorden, Spitsbergen: a geomorphological study of the denudation of slopes in an Arctic locality: Oslo University Press, 96 p.

Reichenbach, P., Galli, M., Cardinali, M., Guzzetti, F., and Ardizzone, F., 2005, Geomorphologic mapping to assess landslide risk: concepts, methods, and applications in the Umbria Region of central Italy, in Glade, T., Anderson, M., and Crozier, M.G., eds., Landslide Risk assessment: Chichester, England, Wiley and Sons, Ltd, doi: 10.1002/9780470012659.ch15.

Rempel, A.W., Wettlaufer, J.S., and Worster, M.G., 2004, Premelting dynamics in a continuum model of frost heave: Journal of fluid mechanics, v. 498, p. 227-244.

Sanderson, F., Bakkehoi, S., Hestnes, E., and Lied, K., 1996, The influence of meteorological factors on the initiation of debris flows, rockfalls, rockslides, and rockmass stability, in Senneset, K., ed., 7th International Symposium on Landslides, p. 97-114.

Silhan, K., Brazdil, R., Panek, T., Dobrovolny, P., Kasickova, L., Tolasz, R., Tursky, O., and Vaclavek, M., 2011, Evaluation of meteorological controls on reconstructed rockfall activity in the Czech Flysch Carpathians: Earth Surface Processes and Landforms, v. 36, issue 14, p. 18987-1909.

Silverman, B.W., 1986, Density Estimation for Statistics and Data Analysis: London, Chapman and Hall/CRC, 177 p.

Stock, G.M., Collins, B.D., Santaniello, D.J., Zimmer, V.I., Wieczorek, G.F., and Snyder, J.B., 2013, Historical rock falls in Yosemite National Park, California (1857-2011): U.S. Geological Survey Data Series 746, 17 p., http/pubs.usgs.gov/ds/746.

Varnes, D.J., and International Association of Engineering Geology Commission on Landslides and other Mass Movements on Slopes, 1984, Landslide Hazard Zonation: A Review of Principles and Practice: The UNESCO Press, Paris, 63 p.

Walder, J., and Hallett, B., 1985, A theoretical model of the fracture of rock during freezing: Geological Society of America Bulletin, v. 96, p. 336-346.

Wang, X., Zhang, L., Ding, J., Meng, Q., Iqbal, J., Li, L, and Yang, Z., 2014, Comparison of rockfall susceptibility assessment at local and regional scale: a case study in the north of Beijing (China): Environmental Earth Sciences, v. 72, p. 4639-4652, doi:10.1007/s12665-014-3718-3.

Wellman, H.W., and Wilson, A.T., 1965, Salt weathering, a neglected geological erosive agent in coastal and arid environments: Nature, v. 205, p. 1097-1098.

Wettlaufer, J.S., and Worster, M.G., 1995, Dynamics of premelted films: Frost heave in a capillary: Physics Review E, v. 51, no. 5, p. 4679-4689.

Wieczorek, G.F, and Jäger, S., 1996, Triggering mechanisms and depositional rates of postglacial slope-movement processes in the Yosemite Valley, California: Geomorphology, v. 15, p. 17-31.

Wilen, L.A., and Dash, J.G., 1995, Frost heave dynamics at a single crystal interface: Physical Review Letters, v. 74, no. 25, p. 5076-5079

Worster, M.G., and Wettlaufer, J.S., 1999, The fluid mechanics of pre-melted liquid films, *in* Shyy, W., ed., Fluid Dynamics at Interfaces: Cambridge, Cambridge University Press, p. 339-351.

Yaalon, D.H., 1970, Parallel stone cracking, a weathering process on desert surfaces: Geological Institute of Bucharest: Technology and Economics, Bulletin, v. 18, p. 107-111.

Yalcin, A., and Bulut, F., 2007, Landslide susceptibility mapping using GIS and digital photogrammetric techniques: as case study from Ardesen (NE-Turkey): Natural Hazards, v. 41, p. 201-226.